JCTC Journal of Chemical Theory and Computation

Article

Cite This: J. Chem. Theory Comput. 2019, 15, 1761−1776

pubs.acs.org/JCTC

In Situ Measure of Intrinsic Bond Strength in Crystalline Structures: Local Vibrational Mode Theory for Periodic Systems

Yunwen Tao,[∥,†] Wenli Zou,[‡] Daniel Sethio,[†] Niraj Verma,[†] Yue Qiu,[¶] Chuan Tian,[§] Dieter Cremer,[⊥,†] and Elfi Kraka*[,†]

[†]Department of Chemistry, Southern Methodist University, 3215 Daniel Avenue, Dallas, Texas 75275-0314, United States

[‡]Institute of Modern Physics, Northwest University, Xi'an, Shaanxi 710127, P. R. China

[¶]Grimwade Centre for Cultural Materials Conservation, School of Historical and Philosophical Studies, Faculty of Arts, University of Melbourne, Parkville, Victoria 3052, Australia

[§]Department of Chemistry, Stony Brook University, Stony Brook, New York 11794, United States

ABSTRACT: The local vibrational mode analysis developed by Konkoli and Cremer has been successfully applied to characterize the intrinsic bond strength via local bond stretching force constants in molecular systems. A wealth of new insights into covalent bonding and weak chemical interactions ranging from hydrogen, halogen, pnicogen, and chalcogen to tetrel bonding has been obtained. In this work we extend the local vibrational mode analysis to periodic systems, i.e. crystals, allowing for the first time a quantitative in situ measure of bond strength in the extended systems of one, two, and three dimensions. We present the study of one-dimensional polyacetylene and hydrogen fluoride chains and two-dimensional layers of graphene, water, and melamine-cyanurate as well as three-dimensional ice I_h and crystalline acetone. Besides serving as a new powerful tool for the analysis of bonding in crystals, a systematic comparison of the intrinsic bond strength in periodic systems and that in isolated molecules becomes possible, providing new details into structure and bonding changes upon crystallization. The potential application for the analysis of solid-state vibrational spectra will be discussed.

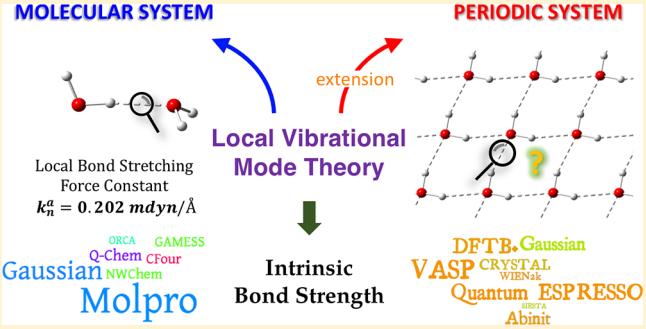

1. INTRODUCTION

The chemical bond is one of the most important concepts in chemistry.[1−4] Chemists often use the bond dissociation energy (BDE) as the measure of bond strength.[5−7] For example, the BDE of the CC single bond in ethane ($H_3C−CH_3$) is 88 kcal/mol, while that of the CC double bond in ethylene ($H_2C═CH_2$) is 174 kcal/mol,[5] reflecting that a CC double bond is stronger than a CC single bond because of additional π bonding. Although the BDE can help chemists to understand chemical bonding in an intuitive way, its deficiencies are obvious. The BDE is a reaction parameter, which involves the overall energy changes of a bond dissociation process. It includes the electron density reorganization and the geometry relaxation of the fragments; therefore, it is not suited as a bond strength descriptor.[6,8] Furthermore, the underlying bond dissociation process into two fragments is not applicable for chemical bonds in complex systems, e.g. large water clusters or metal−organic frameworks (MOFs), in which the dissociation of one bond will drastically change the overall geometry. Therefore, a better alternative to the BDE as bond strength descriptor is desired, that can perform an in situ measure of the bond strength avoiding bond dissociation. Such a bond strength descriptor is expected to reflect all electronic structure factors which are responsible for the bonding mechanism of the target bond, i.e. it directly relates to the *intrinsic bond strength*.[6,8]

In 2000, Cremer and co-workers proposed the local bond stretching force constant as a novel measure of intrinsic bond strength.[7,9] The local bond stretching force constant k_n^a is derived from the local vibrational modes.[10−13] The local mode force constant k_n^a of a specific bond is the curvature of the potential energy surface (PES) in the direction of this bond with its infinitesimal stretching followed by the relaxation of all other parts of this molecule.[14] The local vibrational mode theory has been so far successfully applied to characterize the intrinsic bond strength of both covalent bonds[7,8,15,16] and noncovalent interactions including hydrogen,[17−20] halogen,[21] pnicogen,[22] chalcogen,[23] and tetrel bonding[24] as well as atom···π interactions.[25,26] Local stretching force constants were applied to quantify the intrinsic bond strength of unusual chemical bonding,[15,16,25] to explain interesting physicochemical properties, e.g. the fact that warm water freezes faster than cold water,[19] and to define new electronic parameters[8,27−29] and rules.[30]

Received: December 19, 2018
Published: February 18, 2019

DOI: 10.1021/acs.jctc.8b01279
J. Chem. Theory Comput. 2019, 15, 1761−1776

Several theoretical tools have been developed to analyze chemical bonding in periodic systems. Vanderbilt and coworkers proposed a method based on maximally localized Wannier functions (MLWF),[31,32] where the band structure is transformed into MLWF-orbitals which are more mathematical and as such do not provide much chemical insight. Crystal orbital Hamiltonian population (COHP)[33] and its predecessor crystal orbital overlap population (COOP)[34,35] offer a k-point-dependent characterization of bonding being able to distinguish bonding from antibonding orbitals. The atoms-in-molecules (AIM) approach,[36−38] which is widely used in both molecular and periodic systems, partitions the electron density into atomic basins and provides the bond path connecting any two bonded atoms. From the bond critical points (BCP) and associated bond paths, various bond properties have been derived for the characterization of bonding in molecules as well as in the crystal environment. Alternative topological analysis methods based on the electrostatic potential were developed.[39−41] Recently, Dunnington and Schmidt succeeded in generalizing the natural bond orbital (NBO) analysis[42,43] to periodic systems.[44] In this way, results for periodic systems obtained from plane-wave density functional theory (PW DFT) can now be interpreted with chemically intuitive localized bonding orbitals, as it has been widely used for molecules.[45,46]

In this work, we extend Konkoli and Cremer's local mode theory[10−13] from molecules to periodic systems with a particular focus on deriving a local mode force constant reflecting the intrinsic strength of a bond/weak chemical interaction in periodic systems, e.g. a hydrogen bond in an ice crystal. As a result, a deeper understanding of crystal bonding will be achieved by a head-to-head comparison of the intrinsic bond strength of chemical bonds in periodic and molecular systems.

The paper is structured in the following way: First, the original local vibrational mode theory is summarized using three different routes of deriving local mode force constants k_n^a for molecules. Based on these routes, the definition of local vibrational modes in periodic systems is worked out, as well as the derivation of the corresponding local mode properties with a focus on the local mode force constant k_n^a. After the Computational Details section, seven examples with different dimensions in periodicity (one-, two-, and three-dimensional) are discussed in the Results and Discussion section. The conclusions, along with some general remarks on the calculation of local mode force constants k_n^a, are given in the last section.

2. METHODOLOGY

2.1. Local Vibrational Modes for Isolated Molecules.

In the following, three different routes for deriving local vibrational modes and related properties for molecular systems are summarized, forming the basis for the extension to periodic systems.

2.1.1. Route I. For any N-atomic molecular system being located at either a local/global minimum or a saddle point of first order on the Born−Oppenheimer potential energy surface, the harmonic normal vibrational modes and frequencies can be calculated by solving the Wilson equation of vibrational spectroscopy[47]

$$\mathbf{f}^x\mathbf{L} = \mathbf{ML\Lambda} \tag{1}$$

where $\mathbf{f}^x$ is the $(3N \times 3N)$ dimensional force constant matrix in Cartesian coordinates. The $(3N \times 3N)$ dimensional diagonal mass matrix $\mathbf{M}$ contains each atom three times to account for the motion in x, y, and z directions. The $(N_{vib} \times N_{vib})$ dimensional diagonal matrix $\mathbf{\Lambda}$ collects the N_{vib} vibrational eigenvalues λ_μ (μ = 1, ..., N_{vib} with $N_{vib} = 3N - K$) where K equals 5 for linear and 6 for nonlinear molecules. The $(3N \times N_{vib})$ dimensional matrix $\mathbf{L}$ collects the corresponding vibrational eigenvectors $\mathbf{l}_\mu$ (μ = 1, ..., N_{vib} with $N_{vib} = 3N - K$) as orthonormal column vectors. Harmonic vibrational frequencies ω_μ in [cm^{-1}] and eigenvalues λ_μ are connected via $\lambda_\mu = 4\pi^2c^2\omega_\mu^2$ where c corresponds to the speed of light.[47]

Eq 1 can be rewritten in terms of N_{vib} normal coordinates Q

$$\mathbf{f}^Q = \mathbf{K} = \mathbf{L}^T\mathbf{f}^x\mathbf{L} \tag{2}$$

where the $(N_{vib} \times N_{vib})$ dimensional force constant matrix $\mathbf{f}^Q = \mathbf{K}$ is expressed in terms of normal coordinates Q. The rectangular matrix $\mathbf{L}$ and its transpose $\mathbf{L}^T$ are applied in eq 2.

The local vibrational mode associated with an internal coordinate q_n can be defined via the Wilson $\mathbf{B}$-matrix,[47] which connects the partial derivatives of q_n with the Cartesian coordinates

$$\mathbf{b}_n = \frac{\partial q_n}{\partial \mathbf{x}} \tag{3}$$

The $3N$-dimensional row vector $\mathbf{b}_n$ converts the N_{vib} vibrational modes collected in $\mathbf{L}$ in Cartesian coordinates into the internal coordinates, with the contributions of $\mathbf{L}$ to the internal coordinate q_n given as

$$\mathbf{d}_n = \mathbf{b}_n\mathbf{L} \tag{4}$$

Row vector $\mathbf{d}_n$ of length of N_{vib} is then used to obtain the local mode vector $\mathbf{a}_n$ associated with the internal coordinate q_n[10]

$$\mathbf{a}_n = \frac{\mathbf{K}^{-1}\mathbf{d}_n^T}{\mathbf{d}_n\mathbf{K}^{-1}\mathbf{d}_n^T} \tag{5}$$

where $\mathbf{a}_n$ is a column vector of length N_{vib}. It can be transformed into Cartesian coordinates via[10,48]

$$\mathbf{a}_n^x = \mathbf{L}\mathbf{a}_n \tag{6}$$

where the superscript x denotes Cartesian coordinate, and column vector $\mathbf{a}_n^x$ has the length of $3N$.

The local mode force constant k_n^a associated with internal coordinate q_n is obtained from eq 7.

$$k_n^a = \mathbf{a}_n^T\mathbf{K}\mathbf{a}_n = (\mathbf{d}_n\mathbf{K}^{-1}\mathbf{d}_n^T)^{-1} \tag{7}$$

The local mode force constant k_n^a has also been named *adiabatic force constant*, where the superscript a (adiabatic) means "relaxed" and the subscript n stands for the internal coordinate q_n leading the local vibration.[10]

The corresponding local mode frequency ω_n^a can be derived via the Wilson $\mathbf{G}$-matrix[47,49]

$$(\omega_n^a)^2 = \frac{1}{4\pi^2c^2}k_n^aG_{nn} \tag{8}$$

where the diagonal element $G_{n,n}$ corresponds to the reduced mass of the local mode $\mathbf{a_n}$.[48]

The local mode force constant k_n^a is in contrast to the local mode frequency ω_n^a mass-independent, thus reflecting the pure electronic effects. This has qualified local mode force constants as unique intrinsic bond strength descriptors.[8,15−20] Also in this work, we will use the local mode force constants k_n^a as the

DOI: 10.1021/acs.jctc.8b01279
J. Chem. Theory Comput. 2019, 15, 1761−1776

targeted local mode property for the description of chemical bonding and/or weak chemical interactions in periodic systems.

2.1.2. Route II. An alternative, simplified approach for the calculation of local mode force constants k_n^a was proposed by Zou, Cremer, and co-workers[48] shown in the following equation

$$\frac{1}{k_n^a} = \mathbf{b}_n(\mathbf{f}^x)^+\mathbf{b}_n^T \tag{9}$$

where $(\mathbf{f}^x)^+$ is the Moore-Penrose inverse of $\mathbf{f}^x$. Eq 9 reveals the fundamental physical nature of the local mode force constant as the curvature of the PES given in a specific direction, defined by an internal coordinate q_n as the leading parameter.[8,14] The derivation of eq 9 starts from substituting $\mathbf{d}_n$ and $\mathbf{K}$ in eq 7 using eqs 4 and 2

$$k_n^a = (\mathbf{d}_n\mathbf{K}^{-1}\mathbf{d}_n^T)^{-1} \tag{10}$$

$$k_n^a = (\mathbf{b}_n\mathbf{L}(\mathbf{L}^T\mathbf{f}^x\mathbf{L})^{-1}(\mathbf{b}_n\mathbf{L})^T)^{-1} \tag{11}$$

$$k_n^a = (\mathbf{b}_n\mathbf{L}(\mathbf{L}^T\mathbf{f}^x\mathbf{L})^{-1}\mathbf{L}^T\mathbf{b}_n^T)^{-1} \tag{12}$$

$$k_n^a = (\mathbf{b}_n\mathbf{L}\mathbf{L}^+(\mathbf{f}^x)^+(\mathbf{L}^T)^+\mathbf{L}^T\mathbf{b}_n^T)^{-1} \tag{13}$$

Based on the properties of the Moore-Penrose inverse, it can be proved that $(\mathbf{L}^T)^+ = (\mathbf{L}^+)^T$, and eq 13 can be rewritten as

$$k_n^a = (\mathbf{b}_n\mathbf{L}\mathbf{L}^+(\mathbf{f}^x)^+(\mathbf{L}^+)^T\mathbf{L}^T\mathbf{b}_n^T)^{-1} \tag{14}$$

then

$$k_n^a = (\mathbf{b}_n\mathbf{L}\mathbf{L}^+(\mathbf{f}^x)^+(\mathbf{b}_n\mathbf{L}\mathbf{L}^+)^T)^{-1} \tag{15}$$

where $\mathbf{L}\mathbf{L}^+$ leads to a projection matrix $\mathbf{P}$ in the dimension of $3N \times 3N$, and $\mathbf{P}$ can span the complete internal vibration space as well as the complete internal coordinate space and the external translations and rotations are automatically projected out.

The Wilson $\mathbf{B}$-matrix row vector $\mathbf{b}_n$ of any internal coordinate q_n can be expressed as a linear combination of N_{vib} row vectors in matrix $\mathbf{L}^+$, which equals $\mathbf{L}^T$, leading to

$$\mathbf{b}_n\mathbf{L}\mathbf{L}^+ = \mathbf{b}_n \tag{16}$$

thus eq 15 can be simplified as

$$k_n^a = (\mathbf{b}_n(\mathbf{f}^x)^+\mathbf{b}_n^T)^{-1} \tag{17}$$

which proves the correctness of eq 9.

Compared with route I, route II has two advantages. (i) The expensive step of obtaining the normal vibrational modes by solving the Wilson equation is no longer necessary for calculating k_n^a. (ii) The physical picture of a local mode force constant is clearly revealed by eq 9.

However, it is important to note that eq 16 contains the implicit prerequisite that the internal vibration space spanned by the N_{vib} normal vibrational modes and the internal coordinate space spanned by a complete nonredundant set of N_{vib} internal coordinates are mathematically equivalent.[14]

2.1.3. Route III. The third approach to calculate local mode force constants is based on an unmass-weighted version of route I, proposed for the first time in this work.

The force constant matrix $\mathbf{f}^x$ in Cartesian coordinates is singular and has N_{vib} nonzero eigenvalues collected in the diagonal matrix $\mathbf{\Lambda}'$

$$\mathbf{f}^x\mathbf{C} = \mathbf{C}\mathbf{\Lambda}' \tag{18}$$

where the $(3N \times N_{vib})$-dimensional matrix $\mathbf{C}$ collects eigenvectors $\mathbf{c}_\mu$ (μ = 1, ..., N_{vib}) as column vectors. Eq 18 can be rewritten into

$$\mathbf{\Lambda}' = \mathbf{C}^T\mathbf{f}^x\mathbf{C} \tag{19}$$

This leads to the $\mathbf{d}_n'$ vector associated with internal coordinate q_n via

$$\mathbf{d}_n' = \mathbf{b}_n\mathbf{C} \tag{20}$$

and the local mode force constant k_n^a can be obtained by

$$k_n^a = (\mathbf{d}_n'(\mathbf{\Lambda}')^{-1}(\mathbf{d}_n')^T)^{-1} \tag{21}$$

which leads to the same result as eqs 7 and 17.

2.2. Extension of Local Vibrational Modes to Periodic Systems. *2.2.1. Definition of Konkoli–Cremer Local Modes for Periodic Systems.* The local vibrational mode theory of Konkoli and Cremer in 1998 derives a local vibration being led by an internal coordinate q_n, e.g. a bond stretching, by assuming that all atoms of the molecule expect the ones engaged in the local vibration are a collection of massless points, which can effortlessly follow the leading vibration.[10−13] An extended periodic system has an infinite number of repeating unit cells that are unchanged when translated by the lattice vectors. Crystallographers define the smallest possible unit cell containing exactly one lattice point as the *primitive cell*.[50] Based on the response of all other primitive cells to a bond stretching within one particular primitive cell, two different possibilities of defining local vibrational modes in periodic systems emerge.

1. When a chemical bond in one primitive cell is changed because of a vibration, the remaining atoms in this cell and all other primitive cells should relax. This is equivalent to characterizing the local mode of a chemical bond in an isolated (nonperiodic) cluster model containing an infinite number of primitive cells. Such a treatment of periodic systems was realized in a cyclic cluster model.[51]
2. The vibration of the chemical bond in this primitive cell is synchronized with all other primitive cells, while all atoms except the atom pairs defining this chemical bond will be relaxed. This implies that local vibrational modes in periodic systems are also periodic.

The first definition is more closely related to the physical picture of local vibrational modes in isolated molecular systems; however, it overlooks the fact that in periodic systems, i.e. crystals, any lattice vibration is a collective motion shared by the atoms of all primitive cells. Besides, in molecular systems the local vibrational modes are the local equivalent of the normal vibrational modes in terms of internal coordinates.[48] In analogy, the local vibrational modes in periodic systems should be the local equivalent of the lattice vibrations. Therefore, possibly 2 is more appropriate and leads to the following definition of local vibrational modes in periodic systems: *A local vibrational mode in a periodic system is a vibration initiated by a specific internal coordinate q_n in all primitive cells, obtained after relaxing all other parts in the periodic system.* Noteworthy is that a distinction should be made between (a) Konkoli−Cremer local vibrational modes in periodic systems and (b) the vibrational modes of an impurity in solids also often termed local modes.[52−55]

DOI: 10.1021/acs.jctc.8b01279
J. Chem. Theory Comput. 2019, 15, 1761−1776

2.2.2. Local Mode Frequencies and Force Constants in Periodic Systems. One major difference between the vibrational frequencies in isolated and periodic systems is that periodic systems may have multiple sets of frequencies depending on the k point being investigated, while there is one and only one set of vibrational frequencies for a molecular system.[56,57] However, there exists only one set of vibrations in periodic systems that can be measured by infrared (IR) and Raman spectroscopy, and this set of vibrations corresponds to the one taken at the Γ point ($\mathbf{q} = \mathbf{0}$).[58,59]

In order to obtain a smooth transition from molecular to periodic systems, one has to relate the molecular vibrations to the periodic vibrations at the Γ point ($\mathbf{q} = \mathbf{0}$). A benefit of doing so is that the force constant matrix can be calculated in a primitive cell model with sufficient sampling of the Brillouin zone instead of using supercells.

If the primitive cell of a periodic system has N atoms, the corresponding force constant matrix $\mathbf{f}_P^x$ is of dimension of $3N \times 3N$. In any one-dimensional (1D) periodic system, the force constant matrix $\mathbf{f}_P^x$ has four zero eigenvalues. Three of them are related to the overall translations in the Cartesian coordinate space, while the fourth eigenvector describes the overall rotation of the system around the principal axis parallel to the basis vector. For a two- or three-dimensional (2D/3D) periodic system, the force constant matrix $\mathbf{f}_P^x$ has and only has three zero eigenvalues corresponding to the three overall translations of the primitive cell.

In the following, it will be discussed which of the three available routes for the calculation of local mode force constants in isolated systems can be applied for the calculation of local force constants in periodic systems.

- Route I relies on the precalculated normal vibrational modes. If this scheme is to be used for periodic systems, one issue concerning the 1D periodic systems should be resolved, which is to derive the Eckart−Sayvetz conditions[60−62] for that rotational mode associated with the fourth zero eigenvalue. However, no solutions in this direction have been reported in the literature so far.
- The underlying prerequisite of route II that the internal vibration space spanned by the N_{vib} normal vibrational modes and the internal coordinate space spanned by a complete nonredundant set of N_{vib} internal coordinates are mathematically equivalent is no longer valid for periodic systems, as the internal vibration space spanned by $3N - 4$ or $3N - 3$ vibrations cannot be completely spanned by $3N - 6$ internal coordinates. Therefore, route II cannot be applied to obtain the local mode force constants in periodic systems either.
- Route III has a more general form compared with the other two routes and therefore can be adapted to calculate the local mode force constants in periodic systems as follows.

The force constant matrix $\mathbf{f}_P^x$ of the primitive cell in Cartesian coordinates has N_{vib} nonzero eigenvalues collected as diagonal elements in matrix $\mathbf{\Lambda}'$.

$$\mathbf{f}_P^x\mathbf{C} = \mathbf{C}\mathbf{\Lambda}' \tag{22}$$

However, in contrast to a molecular system, N_{vib} takes the value of $(3N - 4)$ for 1D periodic systems or $(3N - 3)$ for 2/3-D periodic systems. Matrix $\mathbf{C}$ collects N_{vib} eigenvectors $\mathbf{c}_\mu$ columnwise.

Eq 22 can be rewritten as

$$\mathbf{\Lambda}' = \mathbf{C}^T\mathbf{f}_P^x\mathbf{C} \tag{23}$$

For a specific internal coordinate q_n within the unit cell, the $\mathbf{d}_n'$ vector can be calculated with

$$\mathbf{d}_n' = \mathbf{b}_n\mathbf{C} \tag{24}$$

Thus, the local mode force constant of internal coordinate q_n within the unit cell can be calculated using eq 25 in analogy to the molecular system.

$$k_n^a = (\mathbf{d}_n'(\mathbf{\Lambda}')^{-1}(\mathbf{d}_n')^T)^{-1} \tag{25}$$

The local mode frequency ω_n^a in periodic systems can be calculated with eq 8 with the help of k_n^a.

It is worth noting that the local mode force constants k_n^a in periodic systems are independent of the choice of primitive cell. As long as the model chosen for the calculation is the smallest unit cell with translational symmetry, the local mode force constant k_n^a for a specific internal coordinate q_n within such a unit cell can be unambiguously determined.

In Figure 1, a one-dimensional periodic model system is shown with four atoms in the primitive cell. There are two

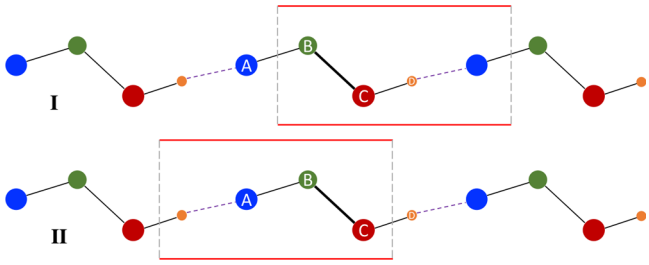

Figure 1. A one-dimensional periodic system with two different choices of primitive cell specified by two rectangles in (I) and (II). Colored circles with labels represent atoms, while black solid and dashed lines indicate chemical bonding.

different possibilities of setting up the primitive cell, labeled with (I) and (II). The boundaries of primitive cell (I) cut through the **A**−**B** bond, the boundaries of primitive cell (II) cut through the **C**−**D** bond, and both cells contain the **B**−**C** bond, which is not broken by any boundary. The force constant matrices calculated for cells (I) and (II) should lead to exactly the same local mode force constants k_n^a for the **B**−**C** bond. This independence of the choice of unit cell for local mode force constants equally applies also to a 2D or 3D periodic system.

If the chemical bond or noncovalent interaction in question is broken by the cell boundaries and not contained within the cell, it is possible to calculate the corresponding local mode force constant k_n^a utilizing translational symmetry. For example, in the 1D periodic system shown in Figure 2, the cell cuts through the **A**−**B** bond on boundaries. As a consequence, there is no **A**−**B** bond defined within this primitive cell, and it seems impossible to calculate the corresponding local mode force constant k_n^a. However, based on eqs 24 and 25, the specification of an internal coordinate q_n, e.g. defining a bond, is decided by the Wilson **B**-vector $\mathbf{b}_n$. The translational symmetry of the primitive cell allows for obtaining the $\mathbf{b}_n$ vector for this **A**−**B** bond by assuming that atom **A** within the cell is shifted into another position at **A**′, which is actually the position of atom **A** of the neighboring cell. $\mathbf{b}_n'$ for bond **A**′−**B**

DOI: 10.1021/acs.jctc.8b01279
J. Chem. Theory Comput. 2019, 15, 1761−1776

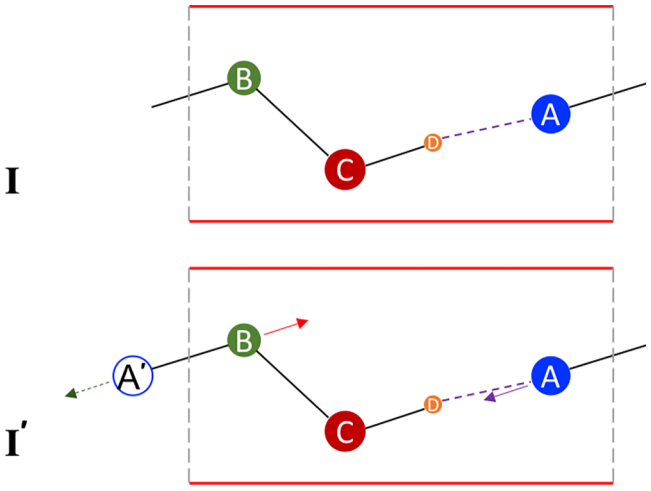

Figure 2. Schematic representation of a one-dimensional periodic system with the primitive cell shown in (I) and the same primitive cell with the atom **A**′ from the neighboring primitive cell shown in (I′).

can be directly used as the $\mathbf{b}_n$ for the bond **A**−**B** cut through by the cell boundaries, i.e. $\mathbf{b}'_n = \mathbf{b}_n$. As the Wilson-**B** vector $\mathbf{b}'_n$ for a bond describes the direction of stretching of two bonded atoms, the stretching direction of atom **A**′ in bond **A**′−**B** can be translated to atom **A** with the help of translational symmetry. In this way, broken bonds cut through by the cell boundaries can still be characterized by local vibrational modes without any extra calculations for a different primitive cell that contains the bond in question. This important property of local mode force constants concerning the primitive cell boundaries also holds for 2D and 3D periodic systems.

One may argue that the local mode force constant k_n^a for a chemical bond in a periodic system may not be directly compared with the local mode force constant of the same type of bond in an isolated molecule, because molecules have five or six translational and rotational modes while periodic systems have only three or four. This argument can be easily refuted as eq 22 reveals that local vibrational modes involve only the vibrational space,[14] and it is physically sound comparing the local mode force constants k_n^a from the vibrational spaces of two systems with a different number of rotations and/or translations, e.g. different periodicity (0−3D).

3. COMPUTATIONAL DETAILS

Geometry optimization including cell relaxation and Hessian evaluation was performed using the Gaussian 16 package[63] for isolated molecules including hydrogen fluoride dimer/hexamer, ethane, ethylene, 1,3,5-hexatriene, benzene, and the melamine−cyanuric acid complex. Periodic boundary conditions (PBC) were employed for periodic systems including a 1D hydrogen fluoride chain, 1D polymers of polyacetylenes (PAs), a 2D monolayer of melamine−cyanuric acid, a 2D graphene layer, and a 3D diamond. The polyacetylenes and their reference molecules were modeled at the B3LYP/6-31G(d,p) level of theory,[64−70] while the hydrogen-bonded systems were calculated with the Minnesota hybrid functional M06-2X with Pople's 6-31+G(d,2p) basis set.[68−71] Due to self-consistent field (SCF) convergence problems arising from the B3LYP hybrid functional, the pure meta-GGA functional of TPSS[72,73] was employed to model 2D graphene, 3D diamond, and their reference molecules using Pople's 6-31G(d,p) basis set.

For the Gaussian 16 calculations, an UltraFine (99,590) integration grid was employed for density functional theory (DFT) calculations, and a tight convergence criteria was achieved for the geometry optimizations. As analytical energy derivatives with regard to Cartesian coordinates are supported only up to the first order in Gaussian 16 for PBC calculations, the Hessian matrix was calculated numerically using four displacements ($\pm\Delta s$, $\pm 2\cdot\Delta s$) for each degree of freedom using analytical gradients, where the step-size Δs of displacement was set to 0.001 Å.

The calculations for the water dimer/hexamer, 2D water monolayer, 3D ice I_h, acetone molecule, and two different forms of acetone crystals were carried out with the CRYSTAL17 program.[74,75] The hydrogen-bonded systems involving water (H_2O) were also modeled with the M06-2X/6-31+G(d,2p) level of theory. The molecule and crystals of acetone were calculated with the same hybrid density functional with Pople's 6-31G(d,p) basis set. In order to achieve optimal accuracy, a pruned XXLGRID (99,1454) integration grid was used, and the two-electron integrals were calculated with the accuracy of 10^{-10}−10^{-12}.

As the CRYSTAL17 program provides analytical energy derivatives with regard to nuclear coordinates and cell parameters only up to the first order (gradients), the Hessian matrices of optimized systems were calculated via numerical differentiation of gradients according to a central-difference formula[76] with a step-size of 0.001 Å.

Noteworthy is that all Hessian matrices used in this work for periodic systems were all evaluated at the Γ point ($\mathbf{q} = \mathbf{0}$) instead of other k-points. This precondition guarantees that the crystal lattice vibrations based on these Hessian matrices are directly measurable by IR or Raman spectroscopy, providing a smooth transition from molecules to periodic systems, e.g. crystals, and an important prerequisite for the discussion of the intrinsic bond strength derived from local vibrational modes.

The local mode analysis including the calculation of adiabatic force constants were carried out with the program package COLOGNE2017.[77] Graphics in Figures 8 were generated by the VESTA3 package.[78]

4. RESULTS AND DISCUSSION

In this section, we discuss local mode force constants k_n^a of chemical bonds and noncovalent interactions in different periodic systems including (i) 1D polymers, (ii) 2D layers, and (iii) 3D crystals.

We also demonstrate how local mode force constants k_n^a used as bond strength descriptors can be directly compared between a periodic and a molecular system or among periodic systems with a different dimension of periodicity gaining deeper insights into chemical bonding.

4.1. 1D Polymers. *4.1.1. Polyacetylene (PA).* Polyacetylene (PA) adopts several different isomers (shown in Figure 3) depending on how the CC double bonds are arranged with regard to each other. The *trans*-PA system was chosen as an ideal model system, often used in modern organic chemistry textbooks when introducing conjugation and π electron delocalization extrapolating stepwise from ethylene, *trans*-1,3-butadiene, etc.[79,80] With an increasing number of C_2H_2 units connected by CC single bonds in a linear chain, the π electron delocalization is expected to enhance and cover more carbon atoms. While various theoretical tools including electron localization function (ELF),[81] localized-orbital locator (LOL),[82] and Mayer bond order[83] have been utilized to

DOI: 10.1021/acs.jctc.8b01279
J. Chem. Theory Comput. 2019, 15, 1761−1776

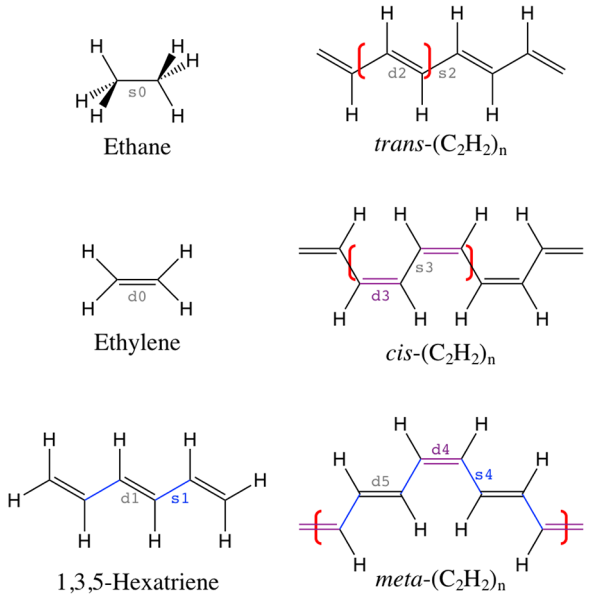

Figure 3. Schematic representation of polyacetylene (PA) isomers including *trans*-PA, *cis*-PA, and *meta*-PA. Brackets colored in red define the primitive cells for calculation. Ethane, ethylene, and 1,3,5-hexatriene are used as references. Single and double carbon−carbon bonds are labeled as (s0)−(s4) and (d0)−(d5), respectively. Symmetry-equivalent single and double bonds are colored in blue and purple.

study the alternating single−double bonds in conjugated alkenes as isolated molecules, there have been only some scattered investigations on the single and double bond strength in PAs as 1D polymers.[84−87] Therefore, we performed a rigorous local mode analysis.

Three PA isomers were calculated including *trans*-, *cis*-, and *meta*-PA with different primitive cells. Ethane, ethylene, and 1,3,5-hexatriene were calculated as references (shown in Figure 3).

Table 1 lists the bond lengths and local mode force constants for the labeled CC single and double bonds in

Table 1. Comparison of Different CC Bonds in Bond Lengths and Local Mode Force Constants for PAs and Reference Molecules

no.	r^a	k_n^{aa}	no.	r^a	k_n^{aa}
		Single Bond			
s0	1.530	4.149	**s1**	1.450	5.279
s2	1.424	5.155	s3	1.436	5.073
s4	1.430	5.374			
		Double Bond			
d0	1.330	9.912	**d1**	1.352	8.623
d2	1.369	6.195	d3	1.369	7.895
d4	1.370	7.530	d5	1.366	7.847

[a]Units for bond length r and local mode force constant k_n^a are Å and mdyn/Å, respectively.

isolated molecules and PAs. Ethane and ethylene are the smallest compounds containing a single and double CC bond, respectively. The double bond (labeled as d0) in ethylene is 0.2 Å shorter than the single bond (s0) in ethane and has a local mode force constant k_n^a as 9.912 mdyn/Å compared with 4.149 mdyn/Å for the single bond (s0). In 1,3,5-hexatriene, the influence arising from the alternating single−double CC bonds on both single and double CC bonds can be characterized. The double bond (d1) in the molecular center is longer and weaker than the ethylene double bond (d0), while the single bond (s1) is shorter and stronger than the ethane single bond (s0). This reveals that due to π electron delocalization, the double bond (d1) has less π electron density concentrated in its bonding region compared with double bond (d0), while the single bond (s1) takes partial double bond character and becomes stronger. The analysis on these three molecular systems confirms that the local mode force constant k_n^a as bond strength descriptor is suitable to characterize the influence of π electron delocalization on the strength of CC bonds.[15] This should also hold for the intrinsic bond strength of CC bonds in PAs characterized with local mode force constants k_n^a.

All four unique double bonds (d2−d5) in the three PA isomers are longer than the reference double bond (d1) and are very close to each other covering a range of 1.366−1.370 Å. Their local mode force constants k_n^a are smaller by 0.728−2.428 mdyn/Å compared with that of double bond (d1), confirming that π electron delocalization is more enhanced in PAs compared to single molecules. The double bond (d2) in *trans*-PA has the smallest local mode force constant k_n^a among three PA isomers. This can be explained by the fact that the polymer chain of *trans*-PA provides the easiest route for electron delocalization in a nearly straight line shape, and therefore the π electrons are more delocalized leading to the weakest double bond (d2). This is in line with the fact that the undoped *trans*-PA has higher electrical conductivity (10^{-5}−10^{-4} S·cm^{-1}) as a semiconductor than undoped *cis*-PA (10^{-10}−10^{-9} S·cm^{-1}) as an insulator.[84,88] The three unique single bonds (s2-s4) in PAs have smaller bond lengths than the reference single bond (s1). The local mode force constants k_n^a in PAs are larger compared with the ethane single bond (s0), but only the k_n^a of single bond (s4) in *meta*-PA is larger than that of the reference single bond (s1).

Quantifying the intrinsic bond strength in polymer systems with local mode force constants k_n^a provides deeper insights on how the repeating units are connected with each other. This knowledge forms an important ingredient for the future rational design of polymer materials with desired physico-chemical properties.

4.1.2. Hydrogen Fluoride (HF) Chain. In solid-state hydrogen fluoride,[89] the hydrogen fluoride molecules are connected by intermolecular F···H hydrogen bonds forming a linear zigzag chain as shown in Figure 4. Focusing on a specific F···H hydrogen bond, the hydrogen bond donor accepts one extra hydrogen bond from the left side, and simultaneously the hydrogen bond acceptor donates one hydrogen bond to the right side. This cooperativity found in intermolecular hydrogen bonding known as the "push−pull" effect[20] strengthens the

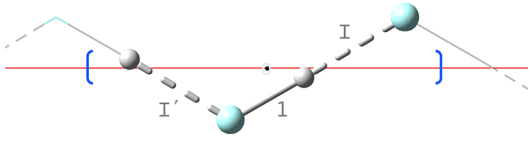

Figure 4. One-dimensional chain of hydrogen fluoride connected by hydrogen bonds. Atoms in the primitive cells are drawn with balls and sticks, where the fluorine and hydrogen atoms are colored in cyan and white, respectively. The covalent F−H bond is labeled with 1, and two symmetry-equivalent F···H hydrogen bonds are labeled with I and I′.

DOI: 10.1021/acs.jctc.8b01279
J. Chem. Theory Comput. 2019, 15, 1761−1776

target hydrogen bond via enhanced charge transfer of lone pair electrons. Therefore, we investigated to what extent this push−pull effect in the solid hydrogen fluoride can make the hydrogen bond stronger.

We characterized the strength of the covalent F−H and F···H hydrogen bonds via the corresponding local mode force constants k_n^a. As references, we used hydrogen fluoride dimer with C_s symmetry containing only one hydrogen bond and a hexamer ring structure with S_6 symmetry containing six equivalent push−pull hydrogen bonds.[20]

Table 2 collects the bond lengths and local mode force constants of FH bonds. In the case of the two molecular

Table 2. Comparison of Different FH Bonds in Bond Lengths and Local Mode Force Constants for 1D Hydrogen Fluoride Chain and Molecular Hydrogen Fluoride Dimer $(HF)_2$ and Hexamer $(HF)_6$

q_n	r^a	k_n^{aa}
1D Chain		
F···H	1.372	0.400
F−H	0.990	2.718
Molecular Dimer (C_s)		
F···H	1.798	0.209
$F-H_{donor}$	0.930	9.094
$F-H_{acceptor}$	0.927	9.398
Molecular Hexamer (S_6)		
F···H	1.402	0.337
F−H	0.983	3.193

[a]Units for bond length r and local mode force constant k_n^a are Å and mdyn/Å, respectively.

reference systems, the push−pull effect shortens the F···H hydrogen bond by 0.396 Å, and the local mode force constant increases by 0.128 mdyn/Å; at the same time, the F−H covalent donor bond is elongated by 0.053 Å, and the local mode force constant k_n^a drops by 6.205 mdyn/Å, reflecting a large bond strength decrease. The fluoride atom in the HF molecule has three lone pairs, and the push−pull effect amplifies the delocalization of these lone pair electrons into the σ^* antibonding orbital of the donor F−H bond.

The F···H hydrogen bond in the 1D HF chain is even shorter than that in the $(HF)_6$ hexamer ring by 0.03 Å and stronger by 0.063 mdyn/Å as revealed by the local mode force constant. The F−H covalent bond is longer and weaker than that in the hexamer by 0.007 Å and 0.474 mdyn/Å, respectively. Therefore, the push−pull strengthening effect arising from the linear arrangement in the 1D chain is stronger compared with the push−pull effect in the hexamer ring.

This example demonstrated that the "push−pull" effect[20] is not a hypothetical model derived from calculations for understanding H-bonds in small molecular clusters which only exist in gas phase, it is a real and important effect, also present in solids.

4.2. 2D Layers. *4.2.1. Graphene.* Graphene is a single atomic 2D layer of 3D graphite. Due to many uncommon properties stemming from its unique honeycomb lattice structure shown in Figure 5, graphene has attracted the attention of material scientists since it was isolated for the first time more than a decade ago.[90−93] Each carbon atom in graphene is sp^2 hybridized. In addition to three σ bonds with neighboring carbons, it has one electron in its p orbital perpendicular to the 2D plane, forming an extented π-bond

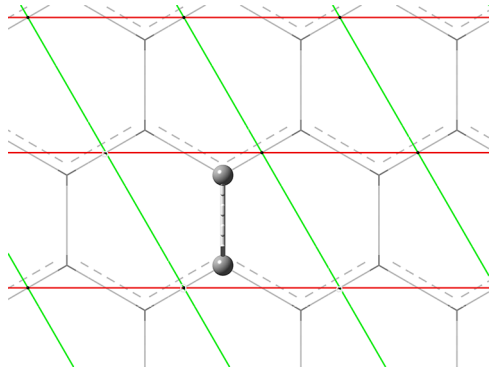

Figure 5. Single layer of graphene where carbon atoms are arranged in a hexagonal lattice structure. Two carbon atoms in the primitive cell are shown as balls and sticks.

over the whole plane. It can be easily deduced that the CC bond strength in graphene is between that of the C−C single bond in ethane and that of the C═C double bond in ethylene.[94] However, it would be helpful to rigorously quantify its intrinsic bond strength in terms of local stretching force constants to be compared with those of other CC bonds.

Bond lengths and local mode force constants for the CC bonds in graphene and reference systems are collected in Table 3. As the B3LYP hybrid functional caused SCF convergence

Table 3. Comparison of Different CC Bonds in Bond Lengths and Local Mode Force Constants for a 2D Graphene Layer and Reference Systems Including Molecular Hydrocarbons and 3D Diamond

system[d]	r^a	k_n^{aa}
graphene	1.429	5.182
ethane	1.535	4.011
1,3,5-hexatriene[b]	1.449	5.200
benzene	1.402	6.446
ethylene	1.336	9.527
diamond[c]	1.552	3.554

[a]Units for bond length r and local mode force constant k_n^a are Å and mdyn/Å, respectively. [b]C−C single bonds in 1,3,5-hexatriene are used in this table for comparison. [c]A primitive cell ($a = b = c = 2.522$ Å, $\alpha = \beta = \gamma = 60°$) containing two carbon atoms converted from a cubic unit cell[95] was used as the starting geometry for the 3D diamond system. [d]Systems listed in this table were all modeled at the TPSS/6-31G(d,p) level of theory.

problems, we switched to the TPSS functional for this example. Compared with the CC bonds in ethane and ethylene, the CC bonds in graphene are in between those two references with regard to both the bond length and local mode force constant. It is noteworthy that the graphene CC bond is longer and weaker than the aromatic CC bond in benzene by 0.027 Å and 1.264 mdyn/Å. Although both benzene and graphene share the hexagonal structure of a C_6 ring, the π electrons in graphene delocalize over a larger space, thus leading to weaker CC bonds. The CC bond strength in graphene is close to that of the single bond in 1,3,5-hexatriene, where the single−double bond alternation renders the single bond with double bond character.

We also included the 3D solid of diamond as a reference system. Diamond has the largest hardness among all natural materials;[96] however, our local mode analysis counter-

DOI: 10.1021/acs.jctc.8b01279
J. Chem. Theory Comput. 2019, 15, 1761−1776

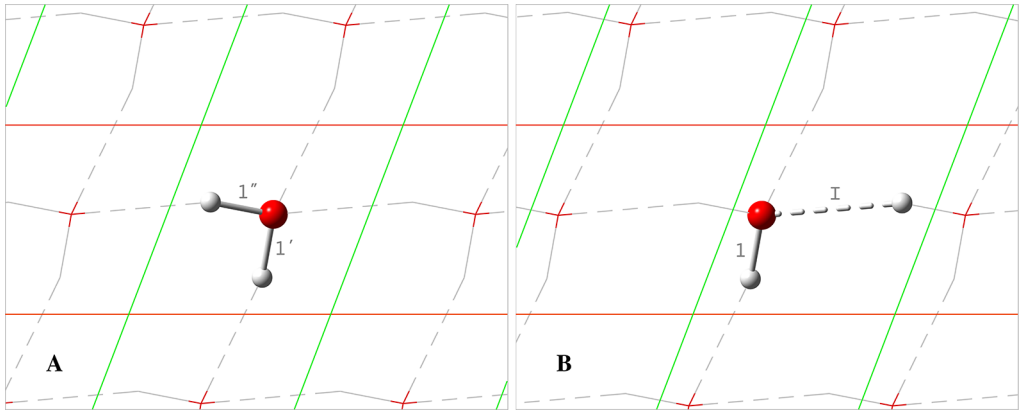

Figure 6. Hydrogen bonding network in a 2D layer formed by water molecules. Two equivalent primitive cells are shown as (A) and (B) in two panels, where the atoms within the primitive cells are shown as balls and sticks. Covalent O−H bonds are labeled with 1, 1′, and 1″, and the O···H hydrogen bond is labeled with I.

intuitively shows that the C−C bond in diamond is the weakest in Table 3. The diamond C−C bond is longer than the ethane C−C bond, and its local stretching force constant is smaller by 0.457 mdyn/Å. A single carbon atom in either diamond or ethane adopts sp^3 hybridization leading to a tetrahedral configuration.[95] The major difference is that the hydrogen atoms in ethane have a weaker capability to attract the bonding electrons in the C−C region compared with the carbon atoms in diamond. This could explain the C−C bond strength differences in these two systems.

In this example, we have quantified the intrinsic bond strengths of CC bonds in 2D graphene as well as 3D diamond for the first time and their ranking among a series of hydrocarbons. Such an analysis could also be applied to another allotrope of carbon, the carbon nanotubes (CNTs).[97] As CNTs can be made with a variety of different structures, the characterization of the CC bond strength in CNTs will be another interesting direction to proceed.

4.2.2. Water. We constructed a model system of water molecules connected with each other in a two-dimensional network as shown in Figure 6. The primitive cell of this system contains only one water molecule, which accepts two hydrogen bonds and donates two hydrogen bonds at the same time to its neighboring water molecules. Noteworthy is that the water molecules are not contained within the plane constructed by the basis vectors, instead the molecule is a little bit tilted with one hydrogen atom above the plane while the other is below the plane for optimal hydrogen bonding configuration. It is interesting that all O−H covalent bonds in this system are equivalent, and all O···H hydrogen bonds have the same bond length as well as local mode force constant due to symmetry.

As references, we used the hydrogen bonding situation in a water dimer structure with C_s symmetry and the push−pull hydrogen bonds in a hexamer water ring with S_6 symmetry,[20] to be compared with the bond strength in the 2D water layer.

Bond lengths and local mode force constants for the three systems are collected in Table 4. When moving from the water dimer to the hexamer ring, one hydrogen bond has its donor water accepting another hydrogen bond and its acceptor water donating another hydrogen bond. This push−pull effect shortens the O···H bond by 0.224 Å and strengthens it by 0.071 mdyn/Å. At the same time, the O−H donor bond is elongated by 0.018 Å, and its local mode force constant decreases by 2.022 mdyn/Å.

Table 4. Comparison of Different OH Bonds in Bond Lengths and Local Mode Force Constants for a 2D Water Layer and Molecular Water Dimer $(H_2O)_2$ and Hexamer $(H_2O)_6$

q_n	r^a	k_n^{aa}
	H_2O 2D Layer	
O···H	1.990	0.681
O−H	0.972	7.748
	H_2O Dimer (C_s)	
O···H	1.925	0.202
$O-H_{donor}$	0.968	8.093
	H_2O Hexamer (S_6)	
O···H	1.701	0.273
$O-H_{donor}$	0.986	6.071

[a]Units for bond length r and local mode force constant k_n^a are Å and mdyn/Å, respectively.

For any O···H hydrogen bond in the 2D water layer, its donor water accepts two external H-bonds and donates one extra H-bond, while its acceptor water donates two H-bonds and accepts one H-bond. According to the push−pull effect, the H-bonds which the donor accepts and the H-bonds the acceptor donates are expected to strengthen the target H-bond. However, the extra H-bonds the donor water donates and the acceptor water accepts are responsible for weakening this target H-bond in question. The result in Table 4 shows that the O···H hydrogen bond in the 2D water layer is longer than that in water dimer but its local mode force constant k^a is larger than the push−pull H-bond in the hexamer ring by 0.408 mdyn/Å. The longer H-bond length accompanied by the larger local mode force constant in the 2D water layer is attributed to the unusual hydrogen bonding configuration where the whole H-bonded network lies almost in a plane. In contrast, common H-bonds in water clusters are almost perpendicular to the acceptor water plane. This local mode force constant k_n^a of 0.681 mdyn/Å for the H-bond is unusual, even larger than the strongest water H-bond with its k_n^a of 0.45 mdyn/Å characterized with a slightly different level of theory in our previous work on water cluster models.[19] This reveals that the strengthening of the H-bond is dominated by the push−pull effect from the four H-bonds which the acceptor donates and the donor accepts. The weakening effect from the other two additional H-bonds which the donor donates and the acceptor accepts is diminished.

DOI: 10.1021/acs.jctc.8b01279
J. Chem. Theory Comput. 2019, 15, 1761−1776

The 2D water layer in this example is a model system which has not been observed so far; however, the local mode analysis can be carried out for other 2D water layer systems which have been observed,[98−100] with the overall objective to discover more unusual H-bonds and in this way to unravel the secrets and peculiarities of water.

4.2.3. Melamine Cyanurate. Melamine cyanurate is a hydrogen bonded complex of melamine and cyanuric acid formed by a 1:1 mixture as solid state.[101] The crystal of melamine cyanurate is composed of layers of hydrogen bonding networks shown in Figure 7. We investigated one

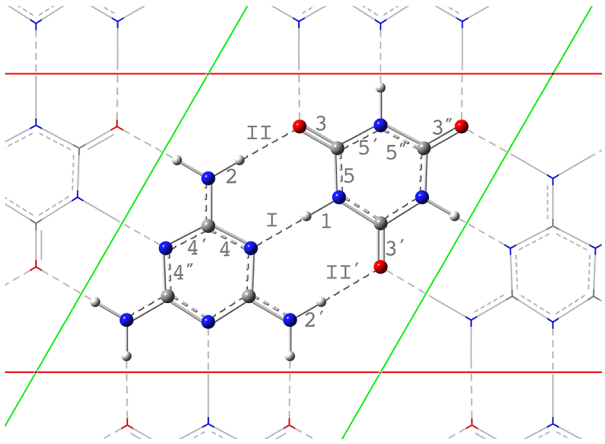

Figure 7. Hydrogen bonding network in a plane formed by a melamine−cyanuric acid complex. Atoms within the primitive cell are shown as balls and sticks. Gray, red, blue, and white colors are for carbon, oxygen, nitrogen, and hydrogen atoms. Covalent bonds are labeled with Arabic numerals, while hydrogen bonds are labeled with Roman numerals.

layer in this work. This 2D periodic system has a primitive cell containing a melamine−cyanuric acid complex connected by three intermolecular hydrogen bonds. All other hydrogen bonds in this system are equivalent to these three due to the D_{3h} symmetry of both the melamine molecule and cyanuric acid molecule. In this 2D hydrogen bond network, hydrogen bonding is coupled with π electron conjugation leading to a unique type of hydrogen bonding called resonance assisted hydrogen bond (RAHB),[102,103] which qualifies it as an interesting target for the local mode analysis.

As a reference, we investigated the molecular melamine−cyanuric acid complex. The melamine−cyanuric acid complex in gas phase is no longer planar; it has a small angle tilted around the central hydrogen bond (labeled with I). Ammonia dimer $(NH_3)_2$ with C_s symmetry was also used as a reference. As Pople's 6-31+G(d,2p) basis set fails to give the correct geometry for the ammonia dimer system, we used 6-31+G(d,p) instead for the dimer as well as the 2D melamine cyanurate network and the melamine−cyanuric acid complex. The results for above systems are listed in Table 5.

We first examined the isolated melamine−cyanuric acid complex in which the melamine and cyanuric acid are connected by three hydrogen bonds including one N···H H-bond and two O···H H-bonds. The local mode force constant value of the O···H_{II} bond is close to that of the H-bond in the water dimer listed in Table 4. The local mode force constant of its donor bond N−H_2 is larger than that of the N−H donor bond in ammonia dimer by 0.275 mdyn/Å. However, the N···H_I bond is stronger than the N···H hydrogen bond in ammonia

Table 5. Comparison of Different Bonds in Bond Lengths and Local Mode Force Constants among the 2D Layer of Melamine Cyanurate, Its Molecular Complex, and Ammonia Dimer[b]

q_n	r^a	k_n^{aa}	q_n	r^a	k_n^{aa}
		2D Layer			
N−H_1	1.057	3.692	O···H_{II}	1.936	0.450
	[1.058]	[3.546]		[1.927]	[0.458]
N−H_2	1.013	7.121	C═O_3	1.225	11.810
	[1.013]	[6.964]	C═N_4	1.349	6.822
N···H_I	1.805	0.430	C═N_5	1.373	6.428
	[1.794]	[0.433]			
		Melamine−Cyanuric Acid Complex (C_2)			
N−H_1	1.072	2.693	O···H_{II}	1.940	0.211
	[1.073]	[2.831]		[1.943]	[0.212]
N−H_2	1.013	7.087	C═O_3	1.217	12.335
	[1.014]	[7.007]	C═$O_{3''}$	1.208	13.184
N···H_I	1.715	0.227	C═N_4	1.352	6.577
	[1.702]	[0.283]	C═$N_{4'}$	1.338	7.028
			C═$N_{4''}$	1.339	7.016
			C═N_5	1.373	6.297
			C═$N_{5'}$	1.384	6.000
			C═$N_{5''}$	1.383	6.058
		Ammonia Dimer (C_s)			
N−H_{donor}	1.020	6.812			
N···H	2.199	0.135			

[a]Units for bond length r and local mode force constant k_n^a are Å and mdyn/Å, respectively. [b]Bond length and local mode force constant values in brackets were obtained with the basis set of 6-31+G(d,2p), while other values were from calculations with the 6-31+G(d,p) basis set.

dimer by 0.092 mdyn/Å. Its donor bond N−H_1 is strikingly weakened by 4.119 mdyn/Å compared with the donor bond in $(NH_3)_2$. An NBO analysis[42,43] on the isolated molecular complex showed that the delocalization energy of lone pair electrons from the acceptor nitrogen atom of the N···H_I bond into the σ^*(N−H_1) antibonding orbital is up to 48 kcal/mol, while the delocalization energy in the ammonia dimer is only 6 kcal/mol. The acceptor nitrogen atom of the N···H_I bond is also within the π conjugated system of the melamine molecule. Therefore, the hydrogen bond N···H_I is identified as a resonance assisted hydrogen bond whose strength is much larger than traditional H-bonds, as reflected by local mode force constant k_n^a.

The flow of π electrons from melamine into cyanuric acid can be characterized by the local mode force constants of the C═N bonds of these two molecules in the complex. In the molecular complex, C═N_4, C═$N_{4'}$, and C═$N_{4''}$ are not symmetry-equivalent. Only the nitrogen atom of C═N_4 accepts the N···H_I hydrogen bond, and its local mode force constant is smaller than the other two by 0.451 and 0.439 mdyn/Å. On the other hand, the C═N_5 bond in the cyanuric acid molecule is stronger than C═$N_{5'}$ and C═$N_{5''}$ by at least 0.239 mdyn/Å. These results confirm the underlying picture that the π electrons of the C═N_4 bond move to the C═N_5 bond region, thus weakening C═N_4 but strengthening C═N_5.

In the primitive cell of the 2D network, either the melamine or the cyanuric acid molecule has now three neighboring molecules. The decrease in the local mode force constant of C═N_4 and the increase for C═N_5 shows a more extended π electron delocalization from melamine to cyanuric acid. This

DOI: 10.1021/acs.jctc.8b01279
J. Chem. Theory Comput. 2019, 15, 1761−1776

leads to a sharp increase in the local mode force constants of N···H_I and O···H_{II} by 0.203 and 0.239 mdyn/Å, respectively. The N−H_1 local mode force constant increases by 0.999 mdyn/Å due to more π electrons on the six-membered ring.

In this example, the local mode analysis was applied for the first time to a resonance assisted H-bond. More systematic investigations on this topic are in progress utilizing the local mode force constant as intrinsic H-bond strength complementing and extending other work.[102,103]

4.3. 3D Crystals. *4.3.1. Ice I_h.* We investigated the ice I_h shown in Figure 8. Ice I_h is the most common crystal form of

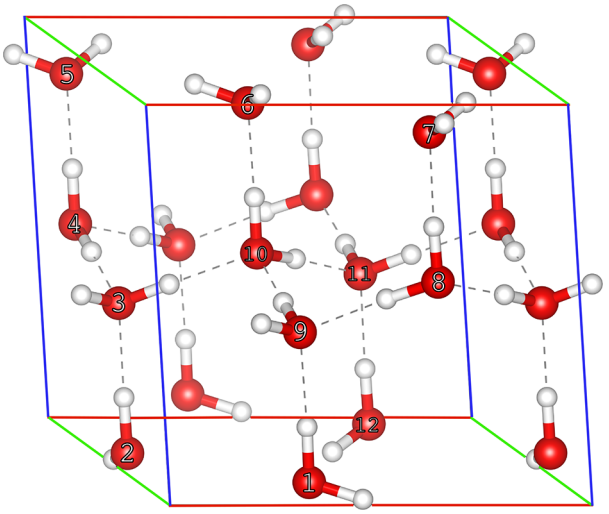

Figure 8. Structure of primitive cell for ice I_h. Red and white balls represent oxygen and hydrogen atoms, respectively. Twelve oxygen atoms contained within the cell are labeled with numbers from 1 to 12, while the unlabeled oxygen atoms are shown as periodic boundary conditions (PBC) images from neighboring cells.

frozen water on earth compared with rare ice I_c which is metastable and only occasionally present.[104] In the ice I_h system, all water molecules are four-coordinated, establishing a hexagonal lattice structure stabilized by H-bonds. While water itself has various peculiar physicochemical properties, it was of interest to quantify the intrinsic bond strengths of O···H hydrogen bonds and O−H covalent donor bonds by the corresponding local mode force constants $k^a_{n,\mathrm{Hb}}$ and $k^a_{n,\mathrm{donor}}$, respectively.

In the resolved crystal structure of ice I_h, all O−H covalent bonds along with the hydrogen bonds they donate can be classified into three categories according to interatomic distance,[105,106] labeled as A, B, and C in Table 6.

The results show that all three different types of O−H covalent bonds and corresponding H-bonds are close to each other in terms of bond lengths and local mode force constants. The donor bond lengths are literally identical as the difference in the fourth digit after the decimal point in Angstroms is largely caused by numerical error from calculation. The deviation in the local mode force constants of covalent bonds in type B and C up to 0.02 mdyn/Å is caused by the calculation of Hessian matrix using numerical differentiation of analytical gradients, and the large size of this primitive cell containing 36 atoms is also responsible. In contrast, although the deviation in the O···H hydrogen bond lengths is relatively larger, their local mode force constants are more close to each other with the maximum deviation of only 0.002 mdyn/Å.

The local mode force constant values of the H-bonds in ice I_h are in the range of 0.252−0.257 mdyn/Å; this means they are stronger than the H-bond in the water dimer (0.202) but weaker than the push−pull H-bond in the hexamer water ring (0.273). Similar to the situation in the 2D water layer (see Figure 6), all water molecules in ice I_h are four-coordinated, namely either the H-bond donor or acceptor donates and accepts two H-bonds at the same time, however, the H-bonds in ice I_h are much weaker compared with those in the 2D layer (0.681). This large difference is caused by different topologies in these two systems. While neighboring water molecules in ice I_h do not have the same orientation, the unique orientation in the 2D water layer facilitates the lone pair charge transfer in a highly directed way, which strengthens the hydrogen bonding.

4.3.2. Acetone. So far, we have discussed several molecular crystals stabilized by intermolecular hydrogen bonding. In the acetone crystal, no hydrogen bonding exists.[107] The dominant driving force to stabilize the lattice structure is the interaction between the dipole moments of acetone molecules.

Acetone (C_{2v} symmetry) has a polar C═O bond where the oxygen atom is more electronegative and accumulates more electron density than the carbon atom.[108] The dipole moment points from the oxygen to the carbon atom. This leads to a special property of acetone, namely if it is placed in an electric field, its C═O bond will always align to the direction of this field and then reorganize its electronic structure. In 1995, Chattopadhyay and Boxer have characterized this phenomenon termed as a vibrational stark effect (VSE) using vibrational spectroscopy.[109] As the C═O bond stretching mode is an intrinsically localized mode, this mode has been then utilized as a probe to measure the strength of vicinal electric field by checking the blue or red shift in vibrational frequency.[110]

In the crystalline structures of acetone shown in Figure 9, the dipole moments of acetones are either parallel or antiparallel to each other. A specific acetone molecule is situated in an effective electric field formed by all other acetone molecules. We determined the intrinsic bond strength of the C═O bond in acetone crystals and characterized the influence from dipole−dipole interactions.

Apart from the X-ray crystal structure[107] shown in Figure 9B, we constructed a metastable crystal model shown in Figure 9A. While the primitive cell of crystal B has two acetone

Table 6. Properties of OH Bonds within the Primitive Cell of Ice I_h

type (no.)[b]	r_{Hb}[a,c]	$k^a_{n,\mathrm{Hb}}$[a,c]	r_{donor}[a,c]	$k^a_{n,\mathrm{donor}}$[a,c]
A(6)	1.7343 ± 0.0001	0.255 ± 0.002	0.9859 ± 0.0000	6.096 ± 0.003
B(3)	1.7371 ± 0.0004	0.257 ± 0.001	0.9858 ± 0.0001	6.052 ± 0.023
C(3)	1.7365 ± 0.0010	0.252 ± 0.000	0.9860 ± 0.0000	6.054 ± 0.020

[a]Units for bond length and local force constant are Å and mdyn/Å, respectively. [b]The first column gives three categories of OH bonds followed by the number of this OH bonds in parentheses. [c]r and k^a_n are bond length and local mode force constant of an OH bond. The subscripts of donor and Hb denote the donor O−H bond and O···H hydrogen bond, respectively.

DOI: 10.1021/acs.jctc.8b01279
J. Chem. Theory Comput. 2019, 15, 1761−1776

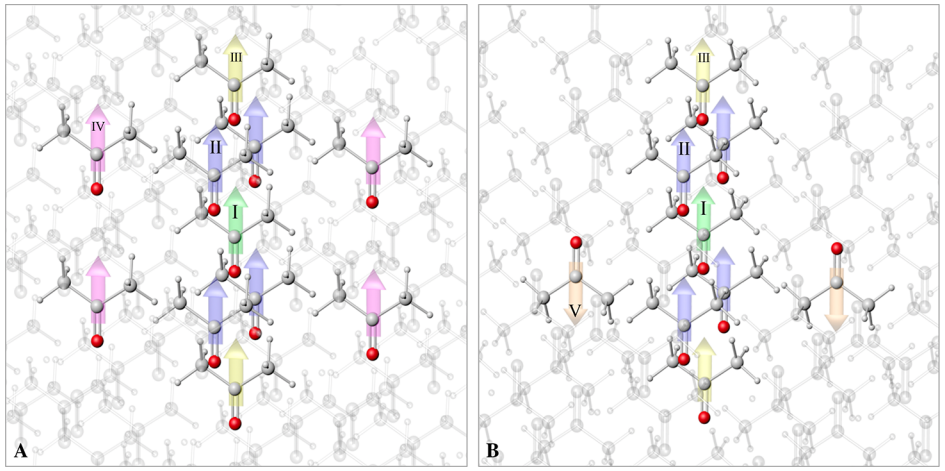

Figure 9. Acetone crystals in two different forms. (A) is a metastable model system, while (B) is a resolved X-ray crystal structure. In either system, the nearby acetone molecules surrounding a target acetone molecule in the center are shown with ball-and-stick models in solid colors. All other acetone molecules are shown with transparent gray color. The dipole moments are represented by arrows in different colors. The target acetone molecule is shown with a green arrow labeled with I.

molecules in an antiparallel orientation, the primitive cell of crystal A contains only one acetone molecule. Therefore, the dipole moments in crystal A are all parallel to each other.

Table 7 lists the bond lengths and local mode force constants of the C═O bonds in the two crystal structures as

Table 7. Comparison of Bond Length r and Local Force Constant k_n^a for the C═O Bond of Acetone in Different Systems

model	r^a	k_n^{aa}
crystal A	1.222	12.542
crystal B	1.224	12.456
molecule	1.209	13.806

[a]Units for bond length r and local mode force constant k_n^a are Å and mdyn/Å, respectively.

well as in the isolated molecule. Acetone has the shortest and strongest C═O bond, while the C═O bond in crystal A is shorter than that in B by 0.002 Å and stronger by 0.086 mdyn/Å.

The reason for the difference in the local mode force constant values is elaborated in the following. In an acetone molecule, excessive electrons are located around the oxygen atom. If an electric field or dipole−dipole interaction polarizes the electrons on the C═O bond toward the oxygen atom, the C═O bond becomes weaker, leading to decreased local mode force constant or the vibrational frequency. If the external electric field polarizes this bond in the other direction, the C═O bond will be stronger.

In the two crystal structures shown in Figure 9, there are in total four different dipole−dipole interactions as shown in Figure 10.

- The first type of dipole−dipole interaction (Figure 10A) denoted as I−II is that the second acetone molecule is located to the front or back of the target acetone and the C═O bonds are in the same plane. This dipole−dipole interaction is found in four surrounding acetones in both crystals. These four molecules with regard to the target acetone are arranged in a staggered manner, leading to the polarization of electrons toward the oxygen atom.

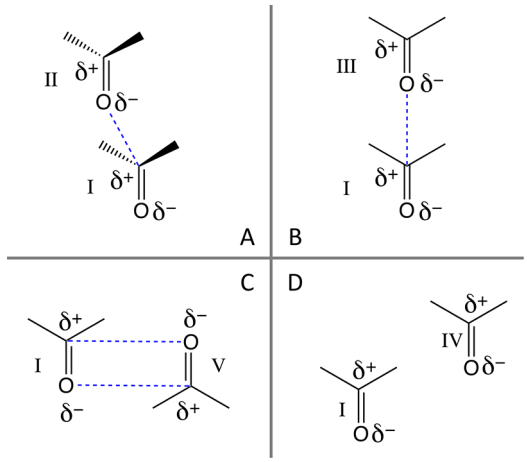

Figure 10. Schematic representation of four different ways of dipole−dipole interaction between acetone molecules.

Therefore, it poses a weakening effect on the C═O bond strength.

- The second type of dipole−dipole interaction (Figure 10B) denoted as I−III is based on the stacking of the second acetone molecule on top of the target acetone or vice versa. This leads to a strong polarization of the excess electrons of the C═O bond toward the oxygen atom because both acetone molecules have their dipole moments in the same line. The C═O bond strength of the target acetone is then reduced.

  Noteworthy is that the arrangement of the acetone molecules resulting in the above two different types of dipole−dipole interaction is the same in both crystals, and these six surrounding molecules are the nearest neighbors of the target acetone in the center. All six molecules weaken the target C═O bond, explaining why the local mode force constants of the C═O bonds in the above two crystals are both smaller than that in molecular acetone.
- The third type of dipole−dipole interaction (Figure 10C) denoted as I−V exists when two acetone molecules sit side by side in an antiparallel orientation

DOI: 10.1021/acs.jctc.8b01279
J. Chem. Theory Comput. 2019, 15, 1761−1776

and both molecules have their heavy atoms in the same plane. Such an interaction has similar polarization effects and weakens the target C═O bond.

- The fourth dipole−dipole interaction (Figure 10D) denoted as I−IV seems similar to the third one; however, two dipole moments are parallel to each other. In this configuration, the electron density of the C═O bond is polarized toward the carbon atom. Thus, this dipole−dipole interaction strengthens the target C═O bond.

If we compare the two crystals with regard to the dipole−dipole interaction, both crystals have I−II and I−III interactions with the same spatial arrangement. The major difference is that crystal A has the I−IV interaction, while crystal B has the I−V interaction instead. All three dipole−dipole interactions for crystal B weaken the target C═O bond. In crystal A there are two dominant weakening dipole−dipole interactions (I−II and I−III) and one type of strengthening dipole−dipole interaction (I−IV) which cancels a small portion of the other two dipole−dipole interactions. This explains why the C═O bonds in both crystals are weaker than that in molecules and why the C═O bond in crystal B is weaker than that in crystal A.

5. CONCLUSIONS

In this work, we have presented a novel approach to characterize the intrinsic bond strength of chemical bonding in periodic systems, i.e. crystals, by extending Konkoli and Cremer's local vibrational mode theory[10−13] which was originally proposed to describe vibrations in isolated molecular systems. This important extension allows for the quantification of the strength of chemical bonds as well as noncovalent interactions in systems of different periodic dimensions (1D, 2D, or 3D) as it has been extensively applied to evaluate the intrinsic bond strength of different kinds of chemical bonding covering both covalent bonds[7,8,15,16] and noncovalent interactions[17−20,24,26] in isolated (0D) molecular systems.

For the seven showcase systems with 1D, 2D, and 3D periodicity, we demonstrated how the local mode force constants k_n^a can be used to quantify the intrinsic bond strength of bonds in these systems. We further elucidated how the local mode force constant k_n^a of a chemical bond in a periodic system can be directly compared with the k_n^a of the same type of bond in a molecular system or another periodic system to gain deeper chemical insights.

The extended local vibrational mode theory for periodic systems clearly outperforms other analysis tools for periodic systems in the following aspects:

- The intrinsic bond strength characterized by local vibrational modes in periodic systems can be legitimately compared with chemical bonding in molecular systems;
- The local mode force constant k_n^a derived from the Hessian matrix (second-order derivatives of the energy with respect to Cartesian coordinates) is a suitable and sensitive intrinsic bond strength measure in solids;
- The calculation of local mode force constants k_n^a in periodic systems only requires the optimized lattice structure of the system and its Hessian matrix for the primitive cell. While most first-principle DFT codes based on plane waves (PW)[111−113] and some atomic orbital (AO)-based packages[63,74,114] provide analytical gradients, the Hessian matrix can be calculated in a numerical differentiation approach with sufficient accuracy for obtaining local mode force constant k_n^a. The VASP program[111,115−117] supports the calculation of analytical Hessians with density-functional perturbation theory (DFPT).[118] Unlike other analysis tools based on electronic wave functions[31−35,44] or electron density,[36,37] the calculation of local mode force constant k_n^a is independent from how the wave functions are obtained using either plane waves or atomic orbitals. This makes the local vibrational mode theory generally applicable across different first principle calculation packages. The pairing of local vibrational mode theory with other analysis tools, e.g. periodic NBO,[44] is expected to give even more abundant information on chemical bonding.

In this study, we applied the extended local vibrational mode theory to five molecular crystals and two covalent crystals. Work is in progress (i) to disclose the bonding properties of metallic and ionic crystals and (ii) to develop a new protocol for the analysis of solid-state IR or Raman spectra, i.e. normal mode decomposition into local mode contributions and the relation of normal modes to local modes with the help of an adiabatic connection scheme, which has been successfully applied to molecular systems.[48] With the emerging number of experimental as well as theoretical studies on IR and Raman spectra of crystalline materials,[58,119−122] this project is more than timely.

The local vibrational mode theory can now be applied to gas phase molecules and solids. If one is to extend the local vibrational mode theory to liquids, a major challenge will be to extract an effective Hessian matrix from the molecular dynamics simulation trajectories for a relatively stable molecule or cluster (without bond breaking/forming) within the whole system. As a first step in this direction, vibrational frequencies (i.e., the power spectrum) of liquids are already available via a Fourier transform of the autocorrelation of the particle velocities from simulation trajectories.[123−126]

A few points need to be taken care of as a caveat when applying local vibrational mode theory in periodic systems to describe bond strength. First, the atomic coordinates as well as the primitive cell parameters should be optimized to reach a local minimum on the potential energy surface. Second, local mode force constants k_n^a should be compared between two bonds made up of the same atoms. If two bonds from two different systems are going to be compared with respect to their local mode force constants, these systems should be modeled with the same level of theory for consistency. As we need the primitive cell model for calculating local vibrational modes, the sampling of the Brillouin zone is expected to be sufficient. Additional test calculations with an increasing number of k-points are recommended to make sure that the local mode force constant k_n^a values are converged. For specific programs, the basis set expansion cutoff,[111] real-space cutoff,[127] integral accuracy, or other parameters need to be scrutinized beforehand.

This work introduces a new and unique theoretical tool for characterizing the intrinsic bond strength in periodic systems by extending Konkoli and Cremer's local vibrational mode theory originally proposed for isolated molecules. We expect this contribution can provide a new useful tool for the community of theoretical chemists as well as experimentalists.

DOI: 10.1021/acs.jctc.8b01279
J. Chem. Theory Comput. 2019, 15, 1761−1776

AUTHOR INFORMATION

Corresponding Author

*E-mail: ekraka@smu.edu.

ORCID

Wenli Zou: 0000-0002-0747-2428
Daniel Sethio: 0000-0002-8075-1482
Dieter Cremer: 0000-0002-6213-5555
Elfi Kraka: 0000-0002-9658-5626

Present Address

[‖]Department of Chemistry and Biochemistry, University of Oklahoma, Norman, OK 73019, United States.

Funding

This work was financially supported by the National Science Foundation (Grant 1464906). We thank SMU for providing generous computational resources.

Notes

The authors declare no competing financial interest.
[⊥]Deceased.

ACKNOWLEDGMENTS

Y.T. thanks Mr. Dong Yang and Dr. Hong-Cun Bai for their assistance in setting up VASP and CRYSTAL calculations. Y.T. also thanks Dr. Tian Lu for his constructive suggestions on a few showcase examples.

REFERENCES

(1) Pauling, L. *The Nature of the Chemical Bond and the Structure of Molecules and Crystals: An Introduction to Modern Structural Chemistry*; Cornell University Press: Ithaca, NY, 1960.
(2) *Theoretical Models Of Chemical Bonding Part 2: The Concept Of The Chemical Bond*; Maksic, Z. B., Ed.; Springer Verlag: Berlin, 1990.
(3) *The Chemical Bond: Chemical Bonding Across the Periodic Table*; Frenking, G., Shaik, S., Eds.; Wiley-VCH: New York, 2014.
(4) *The Chemical Bond: Fundamental Aspects of Chemical Bonding*; Frenking, G., Shaik, S., Eds.; Wiley-VCH, New York, 2014; DOI: 10.1002/9783527664658.
(5) Luo, Y.-R. *Comprehensive Handbook of Chemical Bond Energies*; CRC Press: 2007; DOI: 10.1201/9781420007282.
(6) Cremer, D.; Kraka, E. From Molecular Vibrations to Bonding, Chemical Reactions, and Reaction Mechanism. *Curr. Org. Chem.* **2010**, *14*, 1524−1560.
(7) Cremer, D.; Wu, A.; Larsson, A.; Kraka, E. Some Thoughts About Bond Energies, Bond Lengths, and Force Constants. *J. Mol. Model.* **2000**, *6*, 396−412.
(8) Cremer, D.; Kraka, E. Generalization of the Tolman Electronic Parameter: the Metal−ligand Electronic Parameter and the Intrinsic Strength of the Metal−ligand Bond. *Dalton Trans.* **2017**, *46*, 8323−8338.
(9) Kraka, E.; Cremer, D. Dieter Cremer's Contribution to the Field of Theoretical Chemistry. *Int. J. Quantum Chem.* **2019**, *119*, e25849.
(10) Konkoli, Z.; Cremer, D. A New Way of Analyzing Vibrational Spectra. I. Derivation of Adiabatic Internal Modes. *Int. J. Quantum Chem.* **1998**, *67*, 1−9.
(11) Konkoli, Z.; Larsson, J. A.; Cremer, D. A New Way of Analyzing Vibrational Spectra. II. Comparison of Internal Mode Frequencies. *Int. J. Quantum Chem.* **1998**, *67*, 11−27.
(12) Konkoli, Z.; Cremer, D. A New Way of Analyzing Vibrational Spectra. III. Characterization of Normal Vibrational Modes in terms of Internal Vibrational Modes. *Int. J. Quantum Chem.* **1998**, *67*, 29−40.
(13) Konkoli, Z.; Larsson, J. A.; Cremer, D. A New Way of Analyzing Vibrational Spectra. IV. Application and Testing of Adiabatic Modes Within the Concept of the Characterization of Normal Modes. *Int. J. Quantum Chem.* **1998**, *67*, 41−55.
(14) Tao, Y.; Tian, C.; Verma, N.; Zou, W.; Wang, C.; Cremer, D.; Kraka, E. Recovering Intrinsic Fragmental Vibrations Using the Generalized Subsystem Vibrational Analysis. *J. Chem. Theory Comput.* **2018**, *14*, 2558−2569.
(15) Zou, W.; Cremer, D. C_2 in A Box: Determining its Intrinsic Bond Strength for the $X^1\Sigma_g^+$ Ground State. *Chem. - Eur. J.* **2016**, *22*, 4087−4099.
(16) Kalescky, R.; Kraka, E.; Cremer, D. Identification of the Strongest Bonds in Chemistry. *J. Phys. Chem. A* **2013**, *117*, 8981−8995.
(17) Kalescky, R.; Zou, W.; Kraka, E.; Cremer, D. Local Vibrational Modes of the Water Dimer − Comparison of Theory and Experiment. *Chem. Phys. Lett.* **2012**, *554*, 243−247.
(18) Freindorf, M.; Kraka, E.; Cremer, D. A Comprehensive Analysis of Hydrogen Bond Interactions Based on Local Vibrational Modes. *Int. J. Quantum Chem.* **2012**, *112*, 3174−3187.
(19) Tao, Y.; Zou, W.; Jia, J.; Li, W.; Cremer, D. Different Ways of Hydrogen Bonding in Water - Why Does Warm Water Freeze Faster than Cold Water? *J. Chem. Theory Comput.* **2017**, *13*, 55−76.
(20) Tao, Y.; Zou, W.; Kraka, E. Strengthening of Hydrogen Bonding with the Push-Pull Effect. *Chem. Phys. Lett.* **2017**, *685*, 251−258.
(21) Oliveira, V.; Kraka, E.; Cremer, D. Quantitative Assessment of Halogen Bonding Utilizing Vibrational Spectroscopy. *Inorg. Chem.* **2017**, *56*, 488−502.
(22) Setiawan, D.; Kraka, E.; Cremer, D. Strength of the Pnicogen Bond in Complexes Involving Group Va Elements N, P, and As. *J. Phys. Chem. A* **2015**, *119*, 1642−1656.
(23) Oliveira, V.; Cremer, D.; Kraka, E. The Many Facets of Chalcogen Bonding: Described by Vibrational Spectroscopy. *J. Phys. Chem. A* **2017**, *121*, 6845−6862.
(24) Sethio, D.; Oliveira, V.; Kraka, E. Quantitative Assessment of Tetrel Bonding Utilizing Vibrational Spectroscopy. *Molecules* **2018**, *23*, 2763.
(25) Zhang, X.; Dai, H.; Yan, H.; Zou, W.; Cremer, D. B-H···π Interaction: A New Type of Nonclassical Hydrogen Bonding. *J. Am. Chem. Soc.* **2016**, *138*, 4334−4337.
(26) Zou, W.; Zhang, X.; Dai, H.; Yan, H.; Cremer, D.; Kraka, E. Description of An Unusual Hydrogen Bond Between Carborane and A Phenyl Group. *J. Organomet. Chem.* **2018**, *865*, 114−127.
(27) Tao, Y.; Zou, W.; Cremer, D.; Kraka, E. Correlating the Vibrational Spectra of Structurally Related Molecules: A Spectroscopic Measure of Similarity. *J. Comput. Chem.* **2018**, *39*, 293−306.
(28) Tao, Y.; Zou, W.; Cremer, D.; Kraka, E. Characterizing Chemical Similarity With Vibrational Spectroscopy: New Insights Into the Substituent Effects in Mono-Substituted Benzenes. *J. Phys. Chem. A* **2017**, *121*, 8086−8096.
(29) Verma, N.; Tao, Y.; Marcial, B. L.; Kraka, E. Correlation Between Molecular Acidity (pKa) and Vibrational Spectroscopy. *J. Mol. Model.* **2019**, *25*, 48.
(30) Kalescky, R.; Kraka, E.; Cremer, D. Description of Aromaticity with the Help of Vibrational Spectroscopy: Anthracene and Phenanthrene. *J. Phys. Chem. A* **2014**, *118*, 223−237.
(31) Marzari, N.; Vanderbilt, D. Maximally Localized Generalized Wannier Functions for Composite Energy Bands. *Phys. Rev. B: Condens. Matter Mater. Phys.* **1997**, *56*, 12847−12865.
(32) Souza, I.; Marzari, N.; Vanderbilt, D. Maximally Localized Wannier Functions for Entangled Energy Bands. *Phys. Rev. B: Condens. Matter Mater. Phys.* **2001**, *65*, 035109.
(33) Dronskowski, R.; Bloechl, P. E. Crystal Orbital Hamilton Populations (COHP): Energy-Resolved Visualization of Chemical Bonding in Solids Based on Density-Functional Calculations. *J. Phys. Chem.* **1993**, *97*, 8617−8624.
(34) Hoffman, R. *Solids and Surfaces: A Chemist's View of Bonding in Extended Structures*; Wiley-VCH: 1989.
(35) Hughbanks, T.; Hoffmann, R. Chains of Trans-Edge-Sharing Molybdenum Octahedra: Metal-Metal Bonding in Extended Systems. *J. Am. Chem. Soc.* **1983**, *105*, 3528−3537.

DOI: 10.1021/acs.jctc.8b01279
J. Chem. Theory Comput. 2019, 15, 1761−1776

(36) Bader, R. F. W. *Atoms in Molecules: A Quantum Theory*; Clarendon Press: Oxford, United Kingdom, 1994.
(37) Bader, R. F. W. A Quantum Theory of Molecular Structure and its Applications. *Chem. Rev.* **1991**, *91*, 893−928.
(38) Popelier, P. L. *Atoms in Molecules: An Introduction*; Prentice Hall: 2000.
(39) Leboeuf, M.; Köster, A. M.; Jug, K.; Salahub, D. R. Topological Analysis of the Molecular Electrostatic Potential. *J. Chem. Phys.* **1999**, *111*, 4893−4905.
(40) Andrés, J.; Safont, V. S.; Gracia, L.; Llusar, R.; Longo, E. Bridging Structure and Real-Space Topology: Understanding Complex Molecules and Solid-State Materials. In *Recent Advances in Complex Functional Materials*; Springer International Publishing: 2017; pp 427−454, DOI: 10.1007/978-3-319-53898-3_17.
(41) Otero-de-la-Roza, A.; Johnson, E. R.; Luaña, V. Critic2: A Program for Real-Space Analysis of Quantum Chemical Interactions in Solids. *Comput. Phys. Commun.* **2014**, *185*, 1007−1018.
(42) Weinhold, F.; Landis, C. R. Natural Bond Orbitals and Extensions of Localized Bonding Concepts. *Chem. Educ. Res. Pract.* **2001**, *2*, 91−104.
(43) Foster, J. P.; Weinhold, F. Natural Hybrid Orbitals. *J. Am. Chem. Soc.* **1980**, *102*, 7211−7218.
(44) Dunnington, B. D.; Schmidt, J. R. Generalization of Natural Bond Orbital Analysis to Periodic Systems: Applications to Solids and Surfaces via Plane-Wave Density Functional Theory. *J. Chem. Theory Comput.* **2012**, *8*, 1902−1911.
(45) Weinhold, F.; Landis, C.; Glendening, E. What is NBO analysis and how is it useful? *Int. Rev. Phys. Chem.* **2016**, *35*, 399−440.
(46) Landis, C. R.; Weinhold, F. *The Chemical Bond: Fundamental Aspects of Chemical Bonding*; John Wiley and Sons, Ltd.: 2014; Chapter 3, pp 91−120, DOI: 10.1002/9783527664696.ch3.
(47) Wilson, E. B.; Decius, J. C.; Cross, P. C. *Molecular Vibrations: The Theory of Infrared and Raman Vibrational Spectra*; Dover Publications: Mineola, NY, 2012.
(48) Zou, W.; Kalescky, R.; Kraka, E.; Cremer, D. Relating Normal Vibrational Modes to Local Vibrational Modes with the Help of An Adiabatic Connection Scheme. *J. Chem. Phys.* **2012**, *137*, 084114.
(49) Wilson, E. B. A Method of Obtaining the Expanded Secular Equation for the Vibration Frequencies of A Molecule. *J. Chem. Phys.* **1939**, *7*, 1047−1052.
(50) Tilley, R. J. D. *Crystals and Crystal Structures*; Wiley: 2006.
(51) Janetzko, F.; Köster, A. M.; Salahub, D. R. Development of the Cyclic Cluster Model Formalism for Kohn-Sham Auxiliary Density Functional Theory Methods. *J. Chem. Phys.* **2008**, *128*, 024102.
(52) Fieschi, R.; Nardelli, G. F.; Terzi, N. Local-Mode Frequency Due to Light Substitutional Impurities in Alkali-Halide Crystals: Application to the U Center. *Phys. Rev.* **1965**, *138*, A203−A212.
(53) Nazarewicz, W.; Jurkowski, J. Infrared Absorption by Local Vibrational Modes of Boron Impurities in Germanium. *Phys. Status Solidi B* **1969**, *31*, 237−243.
(54) Sangster, M. J. L.; Harding, J. H. Calculation of Local And Gap Mode Frequencies From Impurities in Alkali Halide. *J. Phys. C: Solid State Phys.* **1986**, *19*, 6153−6167.
(55) Sokolov, V. I.; Gruzdev, N. B.; Farina, I. A. Local Vibrational Mode in Zinc Telluride Associated With A Charged Nickel Impurity. *Phys. Solid State* **2003**, *45*, 1638−1643.
(56) Born, M.; Huang, K. *Dynamical Theory of Crystal Lattices*; Clarendon Press: 1954.
(57) Ferrabone, M.; Baima, J. *Phonon Dispersion with CRYSTAL*; CRYSTAL 2017, 2017.
(58) Pascale, F.; Zicovich-Wilson, C. M.; Gejo, F. L.; Civalleri, B.; Orlando, R.; Dovesi, R. The Calculation of the Vibrational Frequencies of Crystalline Compounds and Its Implementation in the CRYSTAL Code. *J. Comput. Chem.* **2004**, *25*, 888−897.
(59) Civalleri, B.; Pascale, F.; Noel, Y. *Vibrational Frequencies Calculation*; CRYSTAL 2017, 2017.
(60) Eckart, C. Some Studies Concerning Rotating Axes and Polyatomic Molecules. *Phys. Rev.* **1935**, *47*, 552−558.
(61) Sayvetz, A. The Kinetic Energy of Polyatomic Molecules. *J. Chem. Phys.* **1939**, *7*, 383−389.
(62) Szalay, V. Eckart-Sayvetz Conditions Revisited. *J. Chem. Phys.* **2014**, *140*, 234107.
(63) Frisch, M. J.; Trucks, G. W.; Schlegel, H. B.; Scuseria, G. E.; Robb, M. A.; Cheeseman, J. R.; Scalmani, G.; Barone, V.; Petersson, G. A.; Nakatsuji, H.; Li, X.; Caricato, M.; Marenich, A. V.; Bloino, J.; Janesko, B. G.; Gomperts, R.; Mennucci, B.; Hratchian, H. P.; Ortiz, J. V.; Izmaylov, A. F.; Sonnenberg, J. L.; Williams-Young, D.; Ding, F.; Lipparini, F.; Egidi, F.; Goings, J.; Peng, B.; Petrone, A.; Henderson, T.; Ranasinghe, D.; Zakrzewski, V. G.; Gao, J.; Rega, N.; Zheng, G.; Liang, W.; Hada, M.; Ehara, M.; Toyota, K.; Fukuda, R.; Hasegawa, J.; Ishida, M.; Nakajima, T.; Honda, Y.; Kitao, O.; Nakai, H.; Vreven, T.; Throssell, K.; Montgomery, J. A., Jr.; Peralta, J. E.; Ogliaro, F.; Bearpark, M. J.; Heyd, J. J.; Brothers, E. N.; Kudin, K. N.; Staroverov, V. N.; Keith, T. A.; Kobayashi, R.; Normand, J.; Raghavachari, K.; Rendell, A. P.; Burant, J. C.; Iyengar, S. S.; Tomasi, J.; Cossi, M.; Millam, J. M.; Klene, M.; Adamo, C.; Cammi, R.; Ochterski, J. W.; Martin, R. L.; Morokuma, K.; Farkas, O.; Foresman, J. B.; Fox, D. J. *Gaussian 16*, Revision B.01; Gaussian Inc.: Wallingford, CT, 2016.
(64) Becke, A. D. Density-Functional Thermochemistry. III. The Role of Exact Exchange. *J. Chem. Phys.* **1993**, *98*, 5648−5652.
(65) Lee, C.; Yang, W.; Parr, R. G. Development of the Colle-Salvetti Correlation-Energy Formula into A Functional of the Electron Density. *Phys. Rev. B: Condens. Matter Mater. Phys.* **1988**, *37*, 785−789.
(66) Vosko, S. H.; Wilk, L.; Nusair, M. Accurate Spin-Dependent Electron Liquid Correlation Energies for Local Spin Density Calculations: A Critical Analysis. *Can. J. Phys.* **1980**, *58*, 1200−1211.
(67) Stephens, P. J.; Devlin, F. J.; Chabalowski, C. F.; Frisch, M. J. Ab Initio Calculation of Vibrational Absorption and Circular Dichroism Spectra Using Density Functional Force Fields. *J. Phys. Chem.* **1994**, *98*, 11623−11627.
(68) Dill, J. D.; Pople, J. A. Self-Consistent Molecular Orbital Methods. XV. Extended Gaussian-Type Basis Sets for Lithium, Beryllium, and Boron. *J. Chem. Phys.* **1975**, *62*, 2921−2923.
(69) Hehre, W. J.; Ditchfield, R.; Pople, J. A. Self-Consistent Molecular Orbital Methods. XII. Further Extensions of Gaussian-Type Basis Sets for Use in Molecular Orbital Studies of Organic Molecules. *J. Chem. Phys.* **1972**, *56*, 2257−2261.
(70) Hariharan, P. C.; Pople, J. A. The Influence of Polarization Functions on Molecular Orbital Hydrogenation Energies. *Theor. Chem. Acc.* **1973**, *28*, 213−222.
(71) Zhao, Y.; Truhlar, D. G. The M06 Suite of Density Functionals for Main Group Thermochemistry, Thermochemical Kinetics, Noncovalent Interactions, Excited States, and Transition Elements: Two New Functionals and Systematic Testing of Four M06-Class Functionals and 12 Other Functionals. *Theor. Chem. Acc.* **2008**, *120*, 215−241.
(72) Tao, J.; Perdew, J. P.; Staroverov, V. N.; Scuseria, G. E. Climbing the Density Functional Ladder: Nonempirical Meta−Generalized Gradient Approximation Designed for Molecules and Solids. *Phys. Rev. Lett.* **2003**, *91*, 146401.
(73) Haas, P.; Tran, F.; Blaha, P. Calculation of the Lattice Constant of Solids with Semilocal Functionals. *Phys. Rev. B: Condens. Matter Mater. Phys.* **2009**, *79*, 085104.
(74) Dovesi, R.; Erba, A.; Orlando, R.; Zicovich-Wilson, C. M.; Civalleri, B.; Maschio, L.; Rérat, M.; Casassa, S.; Baima, J.; Salustro, S.; Kirtman, B. Quantum-Mechanical Condensed Matter Simulations With CRYSTAL. *Wiley Interdiscip. Rev. Comput. Mol. Sci.* **2018**, *8*, e1360.
(75) Dovesi, R.; Saunders, V. R.; Roetti, C.; Orlando, R.; Zicovich-Wilson, C. M.; Pascale, F.; Civalleri, B.; Doll, K.; Harrison, N. M.; Bush, I. J.; D'Arco, P.; Llunell, M.; Causà, M.; Noël, Y.; Maschio, L.; Erba, A.; Rerat, M.; Casassa, S. *CRYSTAL17 User's Manual*; University of Torino: Torino, 2017.
(76) Boole, G. *A Treatise on the Calculus of Finite Differences*; Cosimo Classics: 2007.

DOI: 10.1021/acs.jctc.8b01279
J. Chem. Theory Comput. 2019, 15, 1761−1776

(77) Kraka, E.; Zou, W.; Filatov, M.; Tao, Y.; Grafenstein, J.; Izotov, D.; Gauss, J.; He, Y.; Wu, A.; Konkoli, Z.; Polo, V.; Olsson, L.; He, Z.; Cremer, D. COLOGNE2017. 2017. See: http://www.smu.edu/catco (accessed Feb 21, 2019).
(78) Momma, K.; Izumi, F. VESTA 3 for Three-Dimensional Visualization of Crystal, Volumetric and Morphology Data. *J. Appl. Crystallogr.* **2011**, *44*, 1272−1276.
(79) Solomons, T. W. G.; Fryhle, C. B.; Snyder, S. A. *Organic Chemistry*, 11th ed.; Wiley: 2013.
(80) McMurry, J. E. *Organic Chemistry*; Brooks Cole: 2011.
(81) Becke, A. D.; Edgecombe, K. E. A Simple Measure of Electron Localization in Atomic and Molecular Systems. *J. Chem. Phys.* **1990**, *92*, 5397−5403.
(82) Jacobsen, H. Localized-Orbital Locator (LOL) Profiles of Chemical Bonding. *Can. J. Chem.* **2008**, *86*, 695−702.
(83) Mayer, I. Bond Order and Valence Indices: A Personal Account. *J. Comput. Chem.* **2007**, *28*, 204−221.
(84) Hudson, B. Polyacetylene: Myth and Reality. *Materials* **2018**, *11*, 242.
(85) Mitsutake, K.; Yano, K.; Tsukada, M. Carrier Localization Suppression by Multipath Transport in Helical Polyacetylene. *J. Phys. Chem. C* **2015**, *119*, 10282−10287.
(86) Vilela, A. F. A.; Gargano, R.; Silva, G. M. E. Linking Model Hamiltonians to ab initio and Semiempirical Methods in Descriptions of Impurities in Conjugated Polymers. *Int. J. Quantum Chem.* **2005**, *103*, 537−542.
(87) Yao, J.; Li, Y.; Zou, Z.; Yang, J.; Yin, Z. First Principles Study of the Electron Transport Through Cis-Polyacetylene Based Molecular Wires. *Phys. B* **2011**, *406*, 3969−3974.
(88) Ehinger, K.; Summerfield, S.; Roth, S. Electrical Conductivity of Polyacetylene: Nonsolitonic Mechanism. *Colloid Polym. Sci.* **1985**, *263*, 714−719.
(89) Johnson, M. W.; Sándor, E.; Arzi, E. The Crystal Structure of Deuterium Fluoride. *Acta Crystallogr., Sect. B: Struct. Crystallogr. Cryst. Chem.* **1975**, *31*, 1998−2003.
(90) Allen, M. J.; Tung, V. C.; Kaner, R. B. Honeycomb Carbon: A Review of Graphene. *Chem. Rev.* **2010**, *110*, 132−145.
(91) Ghuge, A. D.; Shirode, A. R.; Kadam, V. J. Graphene: A Comprehensive Review. *Curr. Drug Targets* **2017**, *18*, 724−733.
(92) Choi, W.; Lahiri, I.; Seelaboyina, R.; Kang, Y. S. Synthesis of Graphene and Its Applications: A Review. *Crit. Rev. Solid State Mater. Sci.* **2010**, *35*, 52−71.
(93) Neto, A. H. C.; Guinea, F.; Peres, N. M. R.; Novoselov, K. S.; Geim, A. K. The electronic properties of graphene. *Rev. Mod. Phys.* **2009**, *81*, 109−162.
(94) Gamboa, A.; Vignoles, G. L.; Leyssale, J.-M. On the Prediction of Graphene's Elastic Properties with Reactive Empirical Bond Order Potentials. *Carbon* **2015**, *89*, 176−187.
(95) Hom, T.; Kiszenik, W.; Post, B. Accurate Lattice Constants From Multiple Reflection Measurements. II. Lattice Constants of Germanium Silicon, and Diamond. *J. Appl. Crystallogr.* **1975**, *8*, 457−458.
(96) Pierson, H. O. *Handbook of Carbon, Graphite, Diamonds and Fullerenes: Processing, Properties and Applications (Materials Science and Process Technology)*; Noyes Publications: 2012.
(97) Tasis, D.; Tagmatarchis, N.; Bianco, A.; Prato, M. Chemistry of Carbon Nanotubes. *Chem. Rev.* **2006**, *106*, 1105−1136.
(98) Mei, H.-X.; Zhang, T.; Huang, H.-Q.; Huang, R.-B.; Zheng, L.-S. Discrete Hexamer Water Clusters and 2D Water Layer Trapped in Three Luminescent Ag/Tetramethylpyrazine/Benzene-Dicarboxylate Hosts: 1D Chain, 2D Layer and 3D Network. *J. Mol. Struct.* **2016**, *1108*, 126−133.
(99) Pezzotti, S.; Galimberti, D. R.; Gaigeot, M.-P. 2D H-Bond Network as the Topmost Skin to the Air−Water Interface. *J. Phys. Chem. Lett.* **2017**, *8*, 3133−3141.
(100) Lakshminarayanan, P. S.; Suresh, E.; Ghosh, P. Formation of an Infinite 2D-Layered Water of $(H_2O)_{45}$ Cluster in a Cryptand-Water Supramolecular Complex: A Template Effect. *J. Am. Chem. Soc.* **2005**, *127*, 13132−13133.
(101) Perdigão, L. M. A.; Champness, N. R.; Beton, P. H. Surface Self-Assembly of the Cyanuric Acid−Melamine Hydrogen Bonded Network. *Chem. Commun.* **2006**, 538−540.
(102) Gilli, G.; Bellucci, F.; Ferretti, V.; Bertolasi, V. Evidence for Resonance-Assisted Hydrogen Bonding From Crystal-Structure Correlations on the Enol Form of the.beta.-diketone Fragment. *J. Am. Chem. Soc.* **1989**, *111*, 1023−1028.
(103) Bertolasi, V.; Gilli, P.; Ferretti, V.; Gilli, G. Evidence for Resonance-Assisted Hydrogen Bonding. 2. Intercorrelation Between Crystal Structure and Spectroscopic Parameters in Eight Intramolecularly Hydrogen Bonded 1, 3-diaryl-1, 3-propanedione Enols. *J. Am. Chem. Soc.* **1991**, *113*, 4917−4925.
(104) Bjerrum, N. Structure and Properties of Ice. *Science* **1952**, *115*, 385−390.
(105) Bernal, J. D.; Fowler, R. H. A Theory of Water and Ionic Solution, with Particular Reference to Hydrogen and Hydroxyl Ions. *J. Chem. Phys.* **1933**, *1*, 515−548.
(106) Pauling, L. The Structure and Entropy of Ice and of Other Crystals with Some Randomness of Atomic Arrangement. *J. Am. Chem. Soc.* **1935**, *57*, 2680−2684.
(107) Allan, D. R.; Clark, S. J.; Ibberson, R. M.; Parsons, S.; Pulham, C. R.; Sawyer, L. The Influence of Pressure and Temperature on the Crystal Structure of Acetone. *Chem. Commun.* **1999**, 751−752.
(108) Pauling, L. The Nature of the Chemical Bond. IV. The Energy of Single Bonds and the Relative Electronegativity of Atoms. *J. Am. Chem. Soc.* **1932**, *54*, 3570−3582.
(109) Chattopadhyay, A.; Boxer, S. G. Vibrational Stark Effect Spectroscopy. *J. Am. Chem. Soc.* **1995**, *117*, 1449−1450.
(110) Fried, S. D.; Boxer, S. G. Measuring Electric Fields and Noncovalent Interactions Using the Vibrational Stark Effect. *Acc. Chem. Res.* **2015**, *48*, 998−1006.
(111) Kresse, G.; Hafner, J. Ab Initio Molecular Dynamics for Liquid Metals. *Phys. Rev. B: Condens. Matter Mater. Phys.* **1993**, *47*, 558−561.
(112) Giannozzi, P.; Andreussi, O.; Brumme, T.; Bunau, O.; Nardelli, M. B.; Calandra, M.; Car, R.; Cavazzoni, C.; Ceresoli, D.; Cococcioni, M.; Colonna, N.; Carnimeo, I.; Corso, A. D.; de Gironcoli, S.; Delugas, P.; DiStasio, R. A.; Ferretti, A.; Floris, A.; Fratesi, G.; Fugallo, G.; Gebauer, R.; Gerstmann, U.; Giustino, F.; Gorni, T.; Jia, J.; Kawamura, M.; Ko, H.-Y.; Kokalj, A.; Küçükbenli, E.; Lazzeri, M.; Marsili, M.; Marzari, N.; Mauri, F.; Nguyen, N. L.; Nguyen, H.-V.; de-la Roza, A. O.; Paulatto, L.; Poncé, S.; Rocca, D.; Sabatini, R.; Santra, B.; Schlipf, M.; Seitsonen, A. P.; Smogunov, A.; Timrov, I.; Thonhauser, T.; Umari, P.; Vast, N.; Wu, X.; Baroni, S. Advanced Capabilities for Materials Modelling With Quantum ESPRESSO. *J. Phys.: Condens. Matter* **2017**, *29*, 465901.
(113) Blaha, P.; Schwarz, K.; Madsen, G. K. H.; Kvasnicka, D.; Luitz, J. *WIEN2K, An Augmented Plane Wave + Local Orbitals Program for Calculating Crystal Properties*; Techn. Universität Wien: Austria, 2001.
(114) Soler, J. M.; Artacho, E.; Gale, J. D.; García, A.; Junquera, J.; Ordejón, P.; Sánchez-Portal, D. The SIESTA Method For ab initio Order-N Materials Simulation. *J. Phys.: Condens. Matter* **2002**, *14*, 2745−2779.
(115) Kresse, G.; Hafner, J. Ab Initio Molecular-Dynamics Simulation of the Liquid-Metal-Amorphous-Semiconductor Transition in Germanium. *Phys. Rev. B: Condens. Matter Mater. Phys.* **1994**, *49*, 14251−14269.
(116) Kresse, G.; Furthmüller, J. Efficiency of Ab-Initio Total Energy Calculations For Metals and Semiconductors Using A Plane-Wave Basis Set. *Comput. Mater. Sci.* **1996**, *6*, 15−50.
(117) Kresse, G.; Furthmüller, J. Efficient Iterative Schemes for Ab Initio Total-Energy Calculations Using A Plane-Wave Basis Set. *Phys. Rev. B: Condens. Matter Mater. Phys.* **1996**, *54*, 11169−11186.
(118) Baroni, S.; de Gironcoli, S.; Corso, A. D.; Giannozzi, P. Phonons and Related Crystal Properties from Density-Functional Perturbation Theory. *Rev. Mod. Phys.* **2001**, *73*, 515−562.
(119) Gentile, F. S.; Salustro, S.; Desmarais, J. K.; Ferrari, A. M.; D'Arco, P.; Dovesi, R. Vibrational Spectroscopy of Hydrogens in

DOI: 10.1021/acs.jctc.8b01279
J. Chem. Theory Comput. 2019, 15, 1761−1776

Diamond: A Quantum Mechanical Treatment. *Phys. Chem. Chem. Phys.* **2018**, *20*, 11930−11940.
(120) Azuri, I.; Hirsch, A.; Reilly, A. M.; Tkatchenko, A.; Kendler, S.; Hod, O.; Kronik, L. Terahertz Spectroscopy of 2,4,6-Trinitrotoluene Molecular Solids From First Principles. *Beilstein J. Org. Chem.* **2018**, *14*, 381−388.
(121) Pandey, A.; Sedova, A.; Daemen, L. L.; Cheng, Y.; Ramirez-Cuesta, A. J. Exposing Key Vibrational Contributions to Properties of Organic Molecular Solids with High Signal, Low Frequency Neutron Spectroscopy and Ab Initio Simulations. *Cryst. Growth Des.* **2018**, *18*, 4815−4821.
(122) Bedoya-Martinez, N.; Giunchi, A.; Salzillo, T.; Venuti, E.; Valle, R. G. D.; Zojer, E. Toward a Reliable Description of the Lattice Vibrations in Organic Molecular Crystals: The Impact of van der Waals Interactions. *J. Chem. Theory Comput.* **2018**, *14*, 4380−4390.
(123) Thomas, M.; Brehm, M.; Fligg, R.; Vöhringer, P.; Kirchner, B. Computing Vibrational Spectra From Ab Initio Molecular Dynamics. *Phys. Chem. Chem. Phys.* **2013**, *15*, 6608.
(124) Mathias, G.; Baer, M. D. Generalized Normal Coordinates for the Vibrational Analysis of Molecular Dynamics Simulations. *J. Chem. Theory Comput.* **2011**, *7*, 2028−2039.
(125) Gaigeot, M.-P.; Martinez, M.; Vuilleumier, R. Infrared Spectroscopy in the Gas and Liquid Phase From First Principle Molecular Dynamics Simulations: Application to Small Peptides. *Mol. Phys.* **2007**, *105*, 2857−2878.
(126) Gastegger, M.; Behler, J.; Marquetand, P. Machine Learning Molecular Dynamics for the Simulation of Infrared Spectra. *Chem. Sci.* **2017**, *8*, 6924−6935.
(127) Delley, B. From Molecules to Solids With the DMol3 Approach. *J. Chem. Phys.* **2000**, *113*, 7756−7764.

DOI: 10.1021/acs.jctc.8b01279
J. Chem. Theory Comput. 2019, 15, 1761−1776